https://doi.org/10.5194/egusphere-2026-6761
Preprint. Discussion started: 11 November 2026
© Author(s) 2026. CC BY 4.0 License.

Measurement report: Molecular composition, size distribution, sources and evolution of organic aerosols in the Sichuan Basin, China–Part I: Non-polar organic compounds

Junke Zhang[1], Yalan Zhou[1], Xunzhe Yao[1], Wei Zhao[1], Siyu Liu[1], Yubao Chen[2], Kai Shi[3], Gehui Wang[2]

[1] School of Environmental Science and Engineering, Southwest Jiaotong University, Chengdu 611756, China
[2] Key Lab of Geographic Information Science of the Ministry of Education, School of Geographic Sciences, East China Normal University, Shanghai 200241, China
[3] College of Environmental Sciences and Engineering, China West Normal University, Nanchong 63700, China

Correspondence to: Junke Zhang (zhangjunke@home.swjtu.edu.cn) and Gehui Wang (ghwang@geo.ecnu.edu.cn)

Abstract. This study measured non-polar organic compounds (NPOCs) in atmospheric particles in two medium-sized cities (Nanchong (NC) and Yibin (YB)) of China's Sichuan Basin across summer and winter. Winter $PM_{2.5}$ concentrations were 3.4 and 3.5 times summer values for NC and YB, respectively, with higher concentrations at YB. Forty-eight NPOCs were identified; their summer concentrations were 1.3 (NC) and 1.6 (YB) times winter levels. The NPOCs were grouped into n-alkanes, PAHs, hopanes, and phthalate esters (PAEs). PAEs dominated NPOCs in summer (71.2%–74.9%), while n-alkanes prevailed in winter (69.6%–76.5%). High summer temperatures favored high PAEs, whereas elevated anthropogenic emissions coupled with adverse meteorology led to increased wintertime n-alkane and PAHs concentrations. Vehicular emissions dominated summer $PM_{2.5}$, accompanied by considerable plastic-related contributions. Secondary inorganic and biomass burning increased in winter, alongside a substantial rise in coal combustion at YB. PAHs, hopanes, and n-alkanes mainly accumulated in fine particles, whereas PAEs were richer in coarse particles. $PM_{2.5}$-bound PAHs posed low health risks in summer and moderate risks in winter. Vehicular emissions contributed nearly half of summer life-time lung cancer risk (LLCR), while coal combustion and biomass burning determined winter LLCR. With worsening pollution, PAEs dominated with rising n-alkanes during YB summer, and n-alkanes became more dominant in winter. Vehicular emissions showed the largest increase and governed $PM_{2.5}$ for YB summer pollution, while winter pollution in both cities was driven by combustion and secondary inorganic sources. Except for hopanes at NC, all NPOCs exhibited particle-size coarsening as pollution worsened in winter.

1 Introduction

In the past few decades, the $PM_{2.5}$ pollution in China has received global attention. Organic aerosols (OA) is a key component of $PM_{2.5}$ (20%-90%), which not only cause deterioration of air quality, but also pose serious risks to human

https://doi.org/10.5194/egusphere-2026-6761
Preprint. Discussion started: 11 November 2026
© Author(s) 2026. CC BY 4.0 License.

health and lead to significant uncertainty in climate change (IPCC, 2023; Wang et al., 2014; Wang et al., 2009). The OA molecular tracers fall into two main categories: non-polar organic compounds (NPOCs) and polar organic compounds. Due to the wide range sources and adverse health effects, NPOCs have attracted widespread attention among OA fractions (Cao et al., 2021; Guo et al., 2024; Han et al., 2018; Haque et al., 2026).

NPOCs primarily consist of n-alkanes, polycyclic aromatic hydrocarbons (PAHs), hopanes, and phthalate esters (PAEs). These substances are widely distributed in the troposphere and originate from well-documented anthropogenic and biogenic sources. The typical sources of n-alkanes include petroleum residues, diesel exhaust, and biomass burning, along with terrestrial plant waxes, fungi, bacteria, and plankton (Fu et al., 2011; Kang et al., 2018). Short- and long-chain n-alkanes derive from distinct sources, which can be identified using indicators including the carbon preference index (CPI) (Geng et al., 2019; Haque et al., 2019). PAHs are predominantly generated during incomplete combustion of organic materials, serving as key tracers for emissions from coal and biomass combustion, vehicle exhaust, and industrial processes (Sun et al., 2022; Liang et al., 2020). Meanwhile, due to their toxicity, PAHs are classified as persistent organic pollutants. Consequently, 16 PAHs have been designated as priority pollutants by the U.S. Environmental Protection Agency (EPA). Moreover, Lin et al. (2016) estimated that approximately 40% of light absorption by water-insoluble brown carbon stems from non-polar to semi-polar organics, including PAHs and their derivatives. Hopanes belong to pentacyclic triterpenoid hydrocarbons, which are predominantly originated from bacteriohopanols embedded within bacterial cell membranes and formed in sedimentary environments through long-term geological evolution. These compounds occur at high concentrations in crude oil and tend to be concentrated in lubricating oil fractions (Haque et al., 2026). Hopanes are highly resistant to environmental degradation, making them reliable biomarkers for tracing fossil fuel-related pollution (Tian et al., 2021). PAEs have been widely used in plastic manufacturing, and they can also be found as a common additive in paints, lubricants, adhesives, packaging, and cosmetics (Gao and Wen, 2016). Attention has been paid to PAEs due to their potential carcinogenic and endocrine disrupting properties (Fu et al., 2008). Combining the distribution characteristics and diagnostic ratios of these NPOCs with multivariate statistical analysis methods, researchers can clarify the emission sources of atmospheric particulate matter, quantify the contributions of anthropogenic and natural sources, and further reveal the potential impacts of these pollutants on regional air quality and public health (Haque et al., 2026).

In addition to the research on single particle sizes (i.e., $PM_{2.5}$, PM_{10}, or TSP), the particle size distribution of NPOCs have also attracted extensive attention. This is because the size-specific distributions of compounds are dependent on their physical-chemical properties, gas-particle partitioning, and photodegradation. Thus characterization of the size-specific distribution of NPOCs is crucial for understanding their formation, assessing their possible environmental fate, health effects, and offering proper management (Kleeman et al., 2008; Wang et al., 2009; Han et al., 2018). Wang et al. (2009) found that

https://doi.org/10.5194/egusphere-2026-6761
Preprint. Discussion started: 11 November 2026
© Author(s) 2026. CC BY 4.0 License.

n-alkane, PAHs, and hopanes were unimodal in most cases, peaking at 0.7–1.1 μm size; in contrast, plant wax derived n-alkanes presented a bimodal distribution with two peaks at the sizes of 0.7–1.1 μm and >4.7 μm in the summer mountain and spring marine samples. Han et al. (2018) found that PAHs and n-alkanes in northeast Chinese cities during autumn and winter were mainly distributed in the 0.56–1.00 μm fraction, while hopanes were associated with the 0.32–1.00 μm fraction, and they highlight the emissions from different aerosol-associated NPOCs origins. Through tunnel observation experiments, Li et al. (2022) found that the distributions of n-alkanes and PAHs exhibited distinct size dependence, while it was expected that the relative abundances and homolog distributions of hopanes were very similar for different size stages.

The Sichuan Basin (SCB) is an emerging economic center in southwest China and one of the most developed and densely populated regions in China. In 2025, this region accounts for 7.2% of the national GDP and 7.7% of the national population. With the growing urbanization and large energy consumption, this area has been suffering from serious air pollution over the past two decades (Luo et al., 2020; Zhang et al., 2025; Zhang et al., 2024b; Song et al., 2022). Despite the air quality in the SCB has significantly improved in recent years, the concentrations of $PM_{2.5}$ over SCB are still higher than the World Health Organization (WHO) Air Quality Guideline (5 μg m^{-3} as an annual average) and the revised Chinese National Ambient Air Quality Standard (CNAAQS, 30 μg m^{-3} as an annual average, GB 3095–2026), especially in winter season (Li et al., 2024; Zhang et al., 2024b; Zhang et al., 2024a; Luo et al., 2019).

In order to gain a deeper understanding of OA in SCB, some scholars have conducted research on the NPOCs in this region. For example, Sun et al. (2022) found that the primary sources of PAHs in winter in Chengdu included biomass burning (20.6%), secondary formation (11.7%), traffic emissions (34.7%), and coal combustion (33.0%). Our recent study found that the concentrations of n-alkanes, PAHs, hopanes, and PAEs in winter of 2023 in Chengdu were 139.9 ± 60.0 ng m^{-3}, 13.3 ± 8.2 ng m^{-3}, 1.3 ± 0.7 ng m^{-3}, and 571.8 ± 246.7 ng m^{-3}, respectively, and anthropogenic sources including biomass burning, vehicular exhaust, and coal combustion were important contributors to NPOCs (Zhang et al., 2025). Liang et al. (2020) found that the concentration of PAHs in Chongqing was 9.7 ± 2.5 ng m^{-3} in summer, much lower than that in winter (49.6 ± 16.5 ng m^{-3}), and daily BaP equivalent concentrations during 97% of the winter campaign exceeded the CNAAQS (2.5 ng m^{-3}). These findings provide important scientific information for understanding the characteristics and impacts of NPOCs in SCB.

However, compared with other polluted regions in China such as the Beijing-Tianjin-Hebei, Yangtze River Delta, and Pearl River Delta, research on NPOCs in the SCB remains severely insufficient. Meanwhile, the previous studies mostly focused on the two megacities in SCB, i.e., Chengdu and Chongqing. However, in addition to these two megacities, there are over a dozen medium-sized cities distributed in this region. Due to the differences in the composition of pollution sources and energy structure among different types of cities, the pollution characteristics inevitably vary between megacities and

https://doi.org/10.5194/egusphere-2026-6761
Preprint. Discussion started: 11 November 2026
© Author(s) 2026. CC BY 4.0 License.

medium-sized cities. Unfortunately, targeted studies on NPOCs across medium-sized urban areas in SCB are still rarely reported. This results in an overall understanding of NPOCs in the SCB remains incomplete. To fill this gap, we selected two representative medium-sized cities in the SCB, namely Nanchong (NC) and Yibin (YB), and conducted synchronous $PM_{2.5}$ sampling campaigns in summer and winter. Meanwhile, in winter, the season with the most severe air pollution, we further collected size-segregated particulate matter samples during both non-polluted and polluted days in the two cities. Then we analyzed the spatiotemporal evolution of NPOCs in the two cities, including their concentration, chemical compositions, sources, particle size distributions, and health hazards of PAHs. Furthermore, our previous work has reported the molecular composition of wintertime OA in Chengdu, one of the megacities in the SCB, yet without in-depth analysis of NPOCs. To directly elucidate the differences in atmospheric pollution (especially NPOCs) between medium-sized cities and megacities within the SCB, we incorporated comparisons with results from Chengdu in parts of the discussion section. This enables our results to better characterize NPOCs pollution across the SCB region.

2 Experimental methods

2.1 Sampling sites

$PM_{2.5}$ sampling was conducted at two representative medium-sized cities across the SCB: NC and YB. These two cities serve as representative cites for the polluted areas of northeastern and southern Sichuan, respectively (Figure 1). The NC sampling site was set on the rooftop of a three-story building (approximately 12 m above ground) at China West Normal University. The YB sampling site belongs to the Yibin Air Pollution Super Observation Station and is located on the roof of a two-story building (approximately 8 m above ground). These two sampling sites are all located in the center of the urban area, and the collected samples can represent their air pollution characteristics.

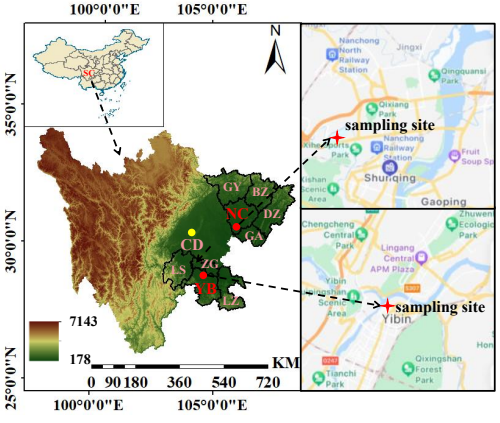


Figure 1: Spatial distribution map of sampling sites (SC: Sichuan Province; CD: Chengdu; NC: Nanchong; YB: Yibin; GY:

https://doi.org/10.5194/egusphere-2026-6761
Preprint. Discussion started: 11 November 2026
© Author(s) 2026. CC BY 4.0 License.

Guangyuan; BZ: Bazhong; DZ: Dazhou; GA: Guang'an; LS: Leshan; ZG:Zigong; LZ: Luzhou; The two site maps on the right are derived from Baidu Maps: https://map.baidu.com/).

2.2 Sample collection

$PM_{2.5}$ sampling was conducted synchronously at both NC and YB during identical summer and winter periods: summer from 15 July to 10 August 2025, and winter from 24 December 2024 to 15 January 2025. The sampler was TH-150F medium-flow sampler (Wuhan Tianhong Instrument Co., Ltd., China), with a sampling flow rate of 100 L min^{-1}. $PM_{2.5}$ samples were collected twice daily (from 08:00 to 19:30 and from 20:00 to 07:30 LT). After excluding sampling failures, 51 and 46 valid $PM_{2.5}$ samples were collected in summer and winter at NC, while 53 and 46 valid $PM_{2.5}$ samples were obtained at YB. In addition, size-segregated aerosols at the two sites in winter under non-polluted (NP) and polluted (P) days were collected by Andersen 8-stage air samplers (Thermoelectronic Company, USA) with the cutoff sizes of 9.0, 5.8, 4.7, 3.3, 2.1, 1.1, 0.65, and 0.43 μm at an airflow rate of 28.3 L min^{-1}. The particle size-resolved aerosols were collected continuously for 3 days per experimental session. Detailed information regarding the pretreatment, weighing, and storage of sampling filters can be found in our previous studies (Wang et al., 2009; Zhang et al., 2025; Cao et al., 2021).

Additionally, meteorological parameters (including ambient temperature, relative humidity (RH), and wind speed) for each site during the study period were downloaded from https://www.aqistudy.cn/. The hourly average concentration data for gaseous pollutants (including CO, SO_2, O_3, and NO_2) at each site were downloaded from the nearest national air quality monitoring station (http://www.cnemc.cn/).

2.3 Chemical analysis

2.3.1 Carbonaceous components and water-soluble inorganic ions

A punch (0.526 cm^2) from each filter sample was analyzed for organic carbon (OC) and elemental carbon (EC) with a DRI model 2001 thermal–optical carbon analyzer (Atmoslytic Inc., Calabasas, CA, USA) following the IMPROVE-A protocol (Chow et al., 2007). Partial filters were cut into pieces and then extracted three times under sonication with 15 mL Milli-Q pure water (18.2 MΩ). Nine ions such as NO_3^-, SO_4^{2-}, Cl^-, F^-, NH_4^+, K^+, Ca^{2+}, Na^+, and Mg^{2+} were determined using ion chromatography (Dionex, ICS-1100) (Huang et al., 2017; Huang et al., 2021; Haque et al., 2019).

2.3.2 OA extraction, derivatization, and GC/MS quantification

Details of the pre-treatment and analysis methods used for OA compounds were described in our previous studies (Zhang et al., 2025; Wang et al., 2009; Wang and Kawamura, 2005). Briefly, filter aliquots were extracted three times with dichloromethane/methanol (2:1, *v*/*v*) under ultrasonication for 10 min. Then the extracts were filtered, concentrated, dried,

https://doi.org/10.5194/egusphere-2026-6761
Preprint. Discussion started: 11 November 2026
© Author(s) 2026. CC BY 4.0 License.

and reacted with N,O-bis(trimethylsilyl)-trifluoroacetamide (BSTFA) with 1% trimethylsilyl chloride and 10 μL of pyridine (5:1, *v*/*v*) at 70 °C for 3 h. Finally, the derivatives were diluted with 140 μL of n-hexane containing 1.43 ng μL^{-1} of the internal standard (C_{13} n-alkane). The pre-treated samples were analyzed by gas chromatography/mass spectrometer (GC/MS) (7890A/5975C, Agilent, USA). Qualitative and quantitative analyses of organic compounds were conducted using literature data, library information, and authentic standards. The response factors of authentic standards or surrogates were used to quantify these organic compounds. The recoveries of the target analytes were obtained by analyzing the spiked quartz filter samples. Most of the recoveries of the spiked standards in the laboratory were 75%-110%. The data reported in this work was corrected by taking account of the field bank, but not the recoveries.

2.4 Data analysis

2.4.1 Health risk assessment

BaP is frequently utilized as an indicator of the carcinogenicity of PAHs due to its toxicity and carcinogenic properties. BaP equivalent concentration (BaP_{eq}) was used to estimate the PAHs associated health risk, and was calculated by the Eq. (1):

$$[BaP_{eq}] = \sum_{i=1}^{n} C_i \times TEF_i \quad (1)$$

where C_i is the concentration of the *i*th PAH (ng m^{-3}). TEF_i is the toxic equivalent factor of the *i*th PAH (Nisbet and Lagoy, 1992).

The life-time lung cancer risk (LLCR) via inhalation was calculated as follows:

$$LLCR = BaP_{eq} \times UR_{BaP} \quad (2)$$

where, BaP_{eq} is estimated by Eq. (1). We have utilized WHO (2000) unit risk (UR) of 8.7×10^{-5} (ng m^{-3})$^{-1}$ (Jia et al., 2011). This means that 8.7 people out of 100,000 people exposed to 1 ng m^{-3} of BaP for 70 years would develop lung cancer.

2.4.2 Positive matrix factorization (PMF) model

Given the strong source-tracing capability of NPOCs, we integrated the measured representative NPOCs species with traditional $PM_{2.5}$ components (carbonaceous and water-soluble inorganic ions) for PMF source apportionment, aiming to obtain more accurate source identification results of $PM_{2.5}$. In this study, the U.S. EPA PMF 5.0 was applied for the source apportionment. Since the categories of atmospheric pollution sources within a given city remain generally stable over a short period, seasonal variations are only reflected in differences in the relative contributions of individual sources. To expand the sample dataset and improve the reliability of results, summer and winter datasets collected at the same monitoring sites were combined for PMF analysis. Specifically, datasets consisting of 97 samples (summer and winter) for NC and 99 samples (summer and winter) for YB were separately adopted to conduct PMF modeling. Species screening for model input was

https://doi.org/10.5194/egusphere-2026-6761
Preprint. Discussion started: 11 November 2026
© Author(s) 2026. CC BY 4.0 License.

conducted according to the signal-to-noise (S/N) ratio proposed by Paatero and Hopke (2003), i.e., the species with S/N ratios below 0.2 were marked as "bad", those ranging from 0.2 to 2 were defined as "weak", and those exceeding 2 were categorized as "strong". Bad species were removed from subsequent modelling, and the uncertainty values of weak species were multiplied by three. Furthermore, to further elucidate the health risks from PAHs sources, PMF was used to apportion LLCR sources. The obtained results can directly reflect the contributions of different sources to LLCR.

3 Results and discussion

3.1 Seasonal variations in air quality and $PM_{2.5}$ chemical composition

As shown in Table 1, atmospheric temperatures at NC and YB were higher in summer and lower in winter, whereas relative humidity exhibited a reversed seasonal trend (higher in winter and lower in summer). Meanwhile, YB featured higher wind speeds than NC throughout the observation period.

Table 1. Overview of meteorological parameters and mass concentrations of pollutants during the observation period.

	NC-summer	NC-winter	YB-summer	YB-winter	CD-winter
T/℃	31.3 ± 4.1	7.5 ± 2.4	29.9 ± 4.0	8.5 ± 2.6	7.2 ± 3.9
RH/%	67.0 ± 17.4	81.0 ± 14.6	72.5 ± 16.2	78.7 ± 14.1	78.2 ± 18.5
WS/m s^{-1}	2.2 ± 1.4	1.9 ± 1.2	3.1 ± 1.6	2.6 ± 1.3	2.3 ± 0.7
$PM_{2.5}$/μg m^{-3}	26.7 ± 10.6	91.7 ± 30.4	37.2 ± 29.0	130.4 ± 36.8	106.5 ± 29.1
CO/mg m^{-3}	0.4 ± 0.1	0.7 ± 0.2	0.8 ± 0.1	0.8 ± 0.1	0.9 ± 0.3
SO_2/μg m^{-3}	5.0 ± 1.4	3.8 ± 0.9	8.8 ± 2.7	9.4 ± 1.1	2.6 ± 0.7
O_3/μg m^{-3}	81.7 ± 38.0	24.0 ± 22.2	88.4 ± 42.2	45.1 ± 26.7	28.2 ± 24.0
NO_2/μg m^{-3}	10.6 ± 5.6	35.0 ± 13.8	13.8 ± 6.1	31.0 ± 9.5	40.9 ± 15.3

The $PM_{2.5}$ concentrations in both NC and YB exhibited higher levels in winter than in summer, with winter concentrations reaching 3.4 and 3.5 times those in summer, respectively. Meanwhile, YB generally had higher $PM_{2.5}$ concentrations than NC; its summer and winter concentrations were both 1.4 times the corresponding seasonal values in NC. Except for NC in summer, the $PM_{2.5}$ levels during the other three observation periods exceeded the revised CNAAQS (30 μg m^{-3} as an annual average, GB 3095–2026). This highlights the severe particulate pollution prevailing in these two medium-sized cities. In terms of winter pollution levels, $PM_{2.5}$ concentrations at NC and YB were 14.8 μg m^{-3} lower and 23.9 μg m^{-3} higher than those at Chengdu, respectively, directly demonstrating the gradual southward aggravation of pollution across the SCB.

For gaseous pollutants, NO_2 exhibited higher concentrations in winter than in summer. By contrast, summer O_3 concentrations at NC and YB were 3.4 and 2.0 times their winter counterparts, respectively. Furthermore, the observed SO_2

https://doi.org/10.5194/egusphere-2026-6761
Preprint. Discussion started: 11 November 2026
© Author(s) 2026. CC BY 4.0 License.

and NO_2 concentrations in these two medium-sized cities were higher and lower than those in Chengdu, respectively, implying stronger coal combustion emissions in the medium-sized cities and greater vehicular emissions in Chengdu.

For $PM_{2.5}$ carbonaceous and ionic components concentrations in two medium-sized cities, all chemical species showed higher winter concentrations except Mg^{2+}, which was more abundant in summer. Figure 2 illustrates the chemical composition of $PM_{2.5}$ at NC and YB. It can be found that OM dominated $PM_{2.5}$ across all observation periods. The highest OM fraction (38.0%) was observed at NC during summer. Meanwhile, the fractional contributions of OM in both cities were higher in summer than in winter. SO_4^{2-} was the most abundant ionic species in summer, accounting for 14.9% and 14.6% at NC and YB, respectively. By contrast, NO_3^- represented the dominant ionic component in winter, contributing 9.7% and 13.8% at NC and YB, respectively. The contributions of secondary inorganic ions in winter in the two medium-sized cities were both lower than the winter observations in Chengdu (Fig. S1), especially for NO_3^- (22.2% in Chengdu). The higher NO_3^- contribution in Chengdu is consistent with the elevated NO_2 concentrations discussed above; meanwhile, such high NO_2 levels can further oxidize SO_2 to form sulfate (Cheng et al., 2016; Huang et al., 2023). In contrast, K^+ exhibited larger contributions in the two medium-sized cities, suggesting stronger biomass burning emissions in medium-sized cities.

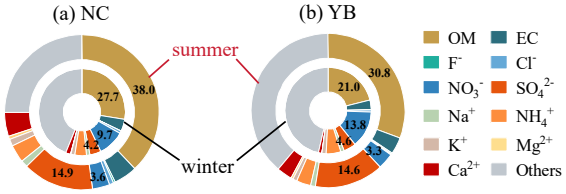


Figure 2: Chemical compositions (%) of $PM_{2.5}$ at NC and YB during summer and winter.

3.2 Chemical composition of NPOCs in $PM_{2.5}$

A total of 48 NPOCs species were identified in $PM_{2.5}$ samples from the two cities. The total NPOCs concentrations at NC were 281.5 ± 91.7 ng m^{-3} in summer and 215.0 ± 117.9 ng m^{-3} in winter, while those at YB were 344.7 ± 143.3 ng m^{-3} in summer and 214.9 ± 125.9 ng m^{-3} in winter. Accordingly, the summer concentrations were approximately 1.3 times and 1.6 times their winter counterparts for NC and YB, respectively. These NPOCs are mainly divided into four categories, namely 19 n-alkanes, 15 PAHs, 11 hopanes, and 3 PAEs. The relative abundances of NPOCs in the two cities are shown in Fig. 3. PAEs were the predominant species in both cities during summer, contributing 71.2% and 74.9% to total NPOCs at NC and YB, respectively. In winter, however, n-alkanes became the most dominant component, accounting for 76.5% at NC and 69.6% at YB. The high proportion of PAEs in summer was mainly caused by elevated ambient temperature, which accelerated the volatilization and release of PAEs into the atmosphere. In contrast, the overwhelming dominance of n-alkanes in winter was primarily driven by intensified combustion emissions, such as biomass burning, coal combustion,

https://doi.org/10.5194/egusphere-2026-6761
Preprint. Discussion started: 11 November 2026
© Author(s) 2026. CC BY 4.0 License.

and vehicle exhaust emissions. This NPOCs composition is comparable to that reported in prior observations at some medium-sized cities. For example, Han et al. (2018) indicated that n-alkanes contributed 67.2% of the total NPOCs in winter in Jiujiang, China. However, Chengdu exhibits a distinctly different NPOCs composition in winter (Fig. S2). Its fractional profile resembled that of the two medium-sized cities in summer, with PAEs dominating absolutely at 77.9%, followed by n-alkanes (20.0%), while PAHs and hopanes only accounted for 2.0% and 0.2%, respectively. In winter, temperature in Chengdu was as low as in the other two cities, suggesting that volatilization may not serve as the dominant PAEs source. The uniquely high level of PAEs was likely associated with abundant emission sources within this megacity, including industrial emissions, plastic waste combustion, urban stock of rubber, plastic building materials, and various indoor plastic commodities. In fact, previous studies on other Chinese megacities such as Guangzhou (Wang et al., 2016) have also observed higher PAEs concentration and contribution in winter than in summer.

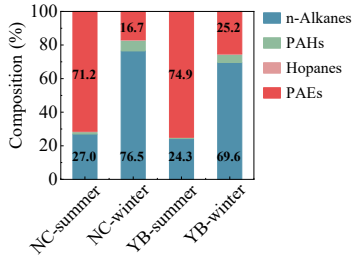


Figure 3: Chemical compositions of NPOCs at NC and YB during summer and winter.

To understand the gas-particle partitioning characteristics of NPOCs in the atmosphere, the particle-phase fraction (φ) of NPOCs was calculated in this study; see S1 for detailed calculation methods. Figure 4 shows the φ of four groups of NPOCs at the two cities. In winter at both sites, the φ values of n-alkanes increased with carbon number, rising from <0.10 for C_{18}–C_{23} to >0.40 for C_{34}–C_{36}. PAHs followed a similar trend: 3-ring species exhibited $\varphi < 0.02$, whereas 5–7-ring congeners had φ exceeding 0.88. Among PAEs, DiBP and DnBP were predominantly present in the gas phase ($\varphi < 0.10$), while DEHP yielded φ values of 0.54–0.56. Hopanes resided almost entirely in the particle phase ($\varphi \approx 1$). Overall φ values in summer were lower than those in winter, yet the relative differences among compound classes remained consistent. Collectively, the measured hopanes and 5–7-ring PAHs in this study can nearly represent their total atmospheric concentrations. For other compounds, the observed concentrations reflected equilibrium gas-particle partitioning modulated by ambient temperature, with lower particle-phase fractions in summer relative to winter.

https://doi.org/10.5194/egusphere-2026-6761
Preprint. Discussion started: 11 November 2026
© Author(s) 2026. CC BY 4.0 License.

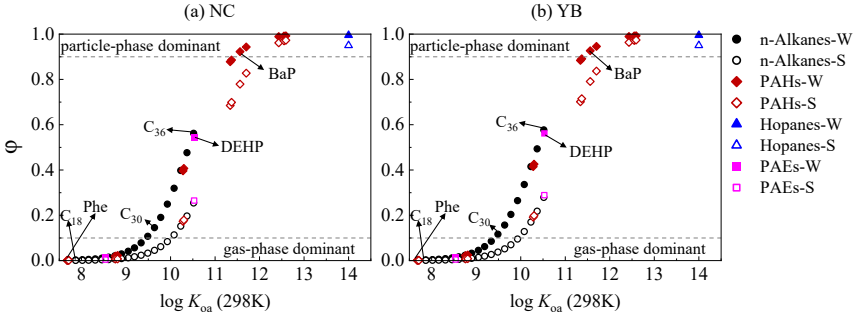


Figure 4: Variations in particle-phase fraction (φ) of NPOCs in NC and YB during summer (S) and winter (W) (Hopanes are plotted at an approximate log K_{oa} of 14 for illustrative purposes. Due to their extremely low volatility, they were assumed to be entirely particle-bound (φ ≈ 1) without applying the temperature-dependent calculation).

3.2.1 n-Alkanes

In this study, n-alkanes in the range of C_{18}-C_{36} were detected. At NC, their concentrations averaged 78.2 ± 36.6 ng m^{-3} in summer and 170.6 ± 105.1 ng m^{-3} in winter, while corresponding values at YB were 91.4 ± 90.5 ng m^{-3} (summer) and 156.1 ± 102.8 ng m^{-3} (winter). Our winter results is slightly higher than the results reported for winter in Chengdu (139.9 ± 60.0 ng m^{-3}), but lower than the results reported in Beijing (286.5 ± 287.8 ng m^{-3}) (Wang et al., 2020), Tianjin (343 ± 227 ng m^{-3} during daytime and 499 ± 307 ng m^{-3} at nighttime) (Fan et al., 2020), and Greater Cairo (653.8 ± 641.2 ng m^{-3}) (Farah et al., 2024). While our summer results is consistent with the summer results in Zhengzhou (89 ± 24 ng m^{-3}) (Wang et al., 2017), but lower than that in Beijing (145.2 ± 80.4 ng m^{-3}) (Wang et al., 2020).

According to previous studies, higher molecular weight (HMW; ≥C_{25}) n-alkanes are originated primarily from continental higher plant waxes, in which C_{29} and C_{31} are major species (Yamamoto and Kawamura, 2010; Fu et al., 2010). Meanwhile, biomass burning can also release HMW n-alkanes, which can lead to HMW n-alkanes carrying mixed signals from natural plant and anthropogenic sources (Yamamoto and Kawamura, 2010; Ren et al., 2016). While lower molecular weight (LMW; < C_{25}) n-alkanes are usually related to anthropogenic activities, such as fossil fuel combustion (Fan et al., 2020; Rogge et al., 1993a). In this study, the HMW/LMW concentration ratios of NC were 2.4 in summer and 4.5 in winter, while those of YB were 2.2 and 4.7, respectively. Correlation analysis found that n-alkanes exhibited strong positive correlations with temperature in summer for both cities, with coefficients of R^2 of 0.58 for NC and 0.68 for YB, respectively. This indicates that elevated concentrations of HMW n-alkanes in summer were likely derived from substantial emissions of continental higher plant waxes under high-temperature conditions. In winter, by contrast, significant positive correlations were observed between n-alkanes and levoglucosan, with R^2 values of 0.46 (NC) and 0.71 (YB), suggesting that biomass burning constituted a critical source of abundant HMW n-alkanes during the cold season.

The CPI value of biogenic n-alkanes is usually greater than unity, while the CPI of anthropogenic n-alkanes is close to 1

https://doi.org/10.5194/egusphere-2026-6761
Preprint. Discussion started: 11 November 2026
© Author(s) 2026. CC BY 4.0 License.

(Rogge et al., 1993b; Simoneit et al., 2004). In this study, CPI values were 1.5 in summer and 2.1 in winter for NC, whereas the corresponding values for YB were 1.5 and 2.0, respectively. This suggests that anthropogenic sources exerted strong control on atmospheric n-alkane abundances. Meanwhile, our observed CPI values are slightly higher than those reported for Zhengzhou (1.3 in summer and 1.2 in winter) (Wang et al., 2017) and Beijing (1.2 in summer and 1.1 in winter) (Wang et al., 2020), implying a larger contribution from anthropogenic sources in these cities of central China and North China.

Calculations of the plant wax n-alkanes contribution (WNA%) showed that the average WNA% was 37.6% in summer and 18.3% in winter at NC, while the corresponding values at YB were 34.7% and 17.8%, respectively. These results imply that n-alkanes at both cities experienced stronger natural source contributions in summer than in winter, which may be associated with high temperatures in summer facilitating their emissions and secondary formation. Meanwhile, our seasonal pattern is consistent with previous observations in Zhengzhou (Wang et al., 2017) and Nanchang (Guo et al., 2024). In contrast, this seasonal variation is opposite to the findings from Guangzhou, where Wang et al. (2016) reported higher WNA% in winter (17.3%) than in summer (12.0%). Differently, Tianjin presented nearly consistent summer and winter WNA% proportions, ranging from 9.9% to 10.2% in summer and 9.0% to 10.1% in winter (Fan et al., 2020). The diverse seasonal variations were closely related to the seasonal changes in anthropogenic sources, vegetation composition, vegetation types, and climatic conditions across different regions (Fu et al., 2010; Guo et al., 2024; Wang et al., 2017).

3.2.2 PAHs

In this study, 15 PAHs were detected in $PM_{2.5}$ from the two cities. Their concentrations were 3.2 ± 1.9 ng m^{-3} in summer and 12.2 ± 5.6 ng m^{-3} in winter at NC, while 2.0 ± 1.6 ng m^{-3} and 9.9 ± 5.5 ng m^{-3} at YB, respectively. The concentrations in winter were 3.8 and 5.0 times those in summer, respectively. Similar seasonal variations have also been observed in other cities, such as Chennai in tropical India (Fu et al., 2010). This can be attributed to elevated emissions and unfavorable meteorological conditions in winter (Wang et al., 2017). Meanwhile, PAHs concentrations in the present study are lower than published data for Chongqing, a megacity in the SCB, with reported seasonal levels of 9.7 ± 2.5 ng m^{-3} in summer and 49.6 ± 16.5 ng m^{-3} in winter (Liang et al., 2020).

Previous studies and our gas-particle partitioning calculations both indicate that 3-ring (low molecular weight (LMW)) PAHs were predominantly presented in the gas phase, 4-ring (medium molecular weight (MMW)) PAHs partition between the gas- and particle-phase, and 5–7-ring (high molecular weight (HMW)) PAHs were predominantly associated with the particle phase (Han et al., 2018; Fu et al., 2008). Consistent with previous observations from Chongqing (Liang et al., 2020), we also observed a higher fraction of MMW PAHs in winter (26.4% at NC, 23.1% at YB) than in summer (9.5% at NC, 14.4% at YB), whereas the opposite seasonal pattern was found for the other two PAHs groups. Beyond seasonal variations in

https://doi.org/10.5194/egusphere-2026-6761
Preprint. Discussion started: 11 November 2026
© Author(s) 2026. CC BY 4.0 License.

source contributions, this discrepancy may also be driven by the semi-volatile property of MMW PAHs, which undergo gas-particle partitioning highly sensitive to ambient temperature. Lower temperatures in winter favor extensive partitioning of MMW PAHs into the particulate phase. In addition, certain MMW species (e.g., BaA) are susceptible to photodegradation and atmospheric oxidation. LMW PAHs are predominantly emitted and enriched in the gas phase in both seasons, while HMW, nearly nonvolatile PAHs tend to remain mostly particle-bound year-round (Liang et al., 2020; Yadav et al., 2024). The seasonal variations of the relative compositions of different PAHs groups are also consistent with the results reported in Wuhan (Zhang et al., 2019) and Hangzhou (Duan et al., 2023).

BaP, considered as the most carcinogenic substance, exhibited average concentrations of 0.2 ± 0.1 ng m^{-3} in summer and 1.0 ± 0.6 ng m^{-3} in winter at NC, and 0.1 ± 0.1 ng m^{-3} and 0.7 ± 0.4 ng m^{-3} at YB, respectively. These concentrations are evidently lower than the observations recorded in winter in the Yangtze River Delta, which were 3.5 ± 1.6 ng m^{-3} for Hangzhou and 2.3 ± 0.7 ng m^{-3} for Nanjing (Cao et al., 2021). Meanwhile, the average concentrations of carcinogenic PAHs (including BaA, Chr, BbF, BkF, BaP, IP, and DBA) were 1.4 ng m^{-3} (summer) and 6.8 ng m^{-3} (winter) at NC, and 0.9 ng m^{-3} (summer) and 5.1 ng m^{-3} (winter) at YB, accounting for 42.1%, 55.8%, 44.9%, and 51.4% of PAHs, respectively. This suggests that, following substantial reductions in atmospheric pollutant emissions in recent years, concentrations of carcinogenic PAHs have decreased markedly, accompanied by a considerable reduction in associated human health risks. Nevertheless, it should not be neglected that carcinogenic PAHs contributed substantially to the total PAHs. A detailed analysis on health risks is presented in Section 3.6.

Combustion-derived PAHs (including Flu, Pyr, BaA, Chr, BbF, BkF, BaP, IP, and BghiP) can be used to determine the influence of combustion source. The average concentrations of combustion-derived PAHs were 1.9 ng m^{-3} (summer) and 9.3 ng m^{-3} (winter) at NC, and 1.2 ng m^{-3} and 7.1 ng m^{-3} at YB, respectively, accounting for 59.0%, 76.5%, 61.6%, and 71.8% of the total PAHs. This highlights the considerable contribution of combustion sources to PAHs in both cities, especially in winter.

The ratios of different PAH species can be used to apportion their sources. Previous studies found that the ratio of IP/BghiP around 0.22, 0.50, and 1.3 are attributable to gasoline, diesel, and coal combustion sources, respectively. While a BghiP/BeP ratio of 2.0 indicates vehicle exhaust and 0.8 indicates coal combustion emissions (Wang et al., 2009; Li et al., 2019). In this study, IP/BghiP ratios were 1.0 (summer) and 1.2 (winter) at NC, compared with 0.9 and 1.1 for summer and winter at YB, respectively. For BghiP/BeP ratios, the corresponding values were 1.7 (summer) and 1.0 (winter) at NC, and 1.2 (summer) and 1.0 (winter) at YB. This indicates that the PAHs in these two medium-sized cities may originate from a mixed source of coal combustion and vehicle exhausts. This can be further verified using the IP/(IP + BghiP) ratio. As reported by Yunker et al. (2002), values of IP/(IP + BghiP) lower than 0.5 point to engine fuel combustion, whereas values exceeding 0.5

https://doi.org/10.5194/egusphere-2026-6761
Preprint. Discussion started: 11 November 2026
© Author(s) 2026. CC BY 4.0 License.

correspond to coal and biomass burning. In our study, the IP/(IP + BghiP) ratio was 0.5 in summer and 0.6 in winter at NC, and stayed at 0.5 in both seasons at YB. This is consistent with the PAHs compositions previously reported for 14 Chinese cities (Wang et al., 2006) and Chennai in tropical India (Fu et al., 2010).

The total index is defined as the sum of some heterogeneous ratios, which is higher than 4.0 when PAHs are generated by high temperature processes (Bootdee et al., 2016; Cao et al., 2021). Our calculated total indexes were 4.2 in summer and 6.9 in winter at NC, as well as 3.9 (summer) and 4.3 (winter) at YB, indicating that PAHs mainly originated from high-temperature combustion processes, which is consistent with our calculated high combustion-derived PAHs values and the results derived from PAHs diagnostic ratios.

In addition to source evaluation, photochemical degradation of PAHs can also be indicated by certain ratios. Photochemical degradation of Ant and BaP is much faster than their structural isomers, Phe and BeP, respectively (Ding et al., 2007). Thus, the Ant/Phe and BaP/BeP ratios are effective indicators reflecting the photochemical processing of PAHs, with values below 1.0 indicates relatively more aged PAHs and the effect of long-range transport. In this study, Ant/Phe ratios averaged 0.1 (summer) and 0.5 (winter) at NC, whereas those at YB were 0.1 for both summer and winter. The BaP/BeP ratios were 0.8 (summer) and 0.9 (winter) at NC, versus 0.6 and 0.7 at YB. These generally low ratios imply that PAHs at both sites underwent substantial photochemical aging, with a greater aging extent observed at YB relative to NC.

3.2.3 Hopanes

Hopanes detected in this study spanned carbon numbers from C_{27} to C_{32}, with the absence of C_{28} homologue. The summed hopanes concentrations at NC averaged 1.2 ± 0.6 ng m^{-3} in summer and 1.4 ± 1.7 ng m^{-3} in winter, while the corresponding values at YB were 0.7 ± 0.3 ng m^{-3} and 0.5 ± 0.2 ng m^{-3}, respectively. Intercity comparison indicated that our hopanes levels are comparable to previously documented concentrations in Chengdu (winter: 1.3 ± 0.7 ng m^{-3}) (Zhang et al., 2025) and Guangzhou (summer: 1.6 ± 0.5 ng m^{-3}, winter: 1.2 ± 0.9 ng m^{-3}) (Wang et al., 2016). While this hopanes abundances are markedly lower than those reported for Beijing (summer: 9.5 ± 5.4 ng m^{-3}, winter: 49.9 ± 36.0 ng m^{-3}) (Wang et al., 2020).

The molecular distribution pattern of hopanes was dominated by the $C_{30}\alpha\beta$ homologue, which exhibited the highest relative abundance: 32.5% (summer) and 28.5% (winter) at NC, and 29.5% (summer) and 26.5% (winter) at YB. $C_{30}\alpha\beta$ is primarily derived from petroleum combustion and lubricating oil release related to motor vehicles. This distribution feature thus reflects the substantial contribution of vehicular emissions to hopanes in both cities. Previous studies have reported that the $C_{29}\alpha\beta/C_{30}\alpha\beta$ ratios corresponding to gasoline, diesel, and coal combustion sources were 0.6–0.7, 0.4, and 0.6–2.0, respectively. Meanwhile, the corresponding $C_{32}\alpha\beta S/(C_{32}\alpha\beta S+C_{32}\alpha\beta R)$ ratios for these three sources were 0.60, 0.60, and 0.2–0.4, respectively (Wang et al., 2009; Oros and Simoneit, 2000). We observed that concentration ratios of $C_{29}\alpha\beta/C_{30}\alpha\beta$ were

https://doi.org/10.5194/egusphere-2026-6761
Preprint. Discussion started: 11 November 2026
© Author(s) 2026. CC BY 4.0 License.

0.6 in summer and 0.9 in winter at NC, as well as 0.8 and 0.7 at YB, respectively. The ratios of $C_{32}\alpha\beta S/(C_{32}\alpha\beta S+C_{32}\alpha\beta R)$ were 0.6 in summer and 0.7 in winter for NC, and 0.6 and 0.6 for YB, respectively. These ratios imply that hopanes in this study were jointly contributed by coal combustion and vehicular emissions.

3.2.4 PAEs

Three PAEs (i.e., DiBP, DnBP, and DEHP) were quantified at NC and YB. Total PAEs concentrations were 199.0 ± 64.0 ng m^{-3} in summer and 30.8 ± 14.7 ng m^{-3} in winter at NC, while the corresponding values at YB were 250.6 ± 84.2 ng m^{-3} and 48.5 ± 23.5 ng m^{-3}, respectively. The summer concentrations were 6.5 and 5.2 times those in winter for NC and YB, respectively. This seasonal pattern is consistent with the results of Fu et al. (2010), who observed higher PAEs concentrations in summer (553 ng m^{-3}) than in winter (303 ng m^{-3}) at Chennai. They attributed the stronger summer emissions to elevated ambient temperatures. In our study, the ambient-temperature dependence of PAEs was supported by the strong correlation between PAEs concentrations and ambient temperature (R^2 were 0.60 at NC and 0.57 at YB). However, an opposite seasonal pattern was observed in Beijing (Wang et al., 2020) and Guangzhou (Wang et al., 2016), where PAEs concentrations were substantially higher in winter than in summer. This discrepancy is likely attributable to the diverse emission pathways of PAEs and regionally dominant emission sources. Apart from volatilization emissions, other processes including industrial production, plastic combustion, photodegradation, regional transmission, and wet and dry deposition can also modulate atmospheric PAEs concentrations (Wang et al., 2016; Fu et al., 2012; Fu et al., 2010). Furthermore, our calculations revealed that the particle-phase fractions of various PAEs in both cities decreased in summer relative to winter. For instance, at NC, the φ values of DiBP and DnDP were 0.012 in winter and 0.004 in summer, while those of DEHP were 0.54 and 0.26 for winter and summer, respectively. At YB, the φ values of DiBP and DnDP were 0.014 in winter and 0.004 in summer, with DEHP showing values of 0.56 (winter) and 0.29 (summer). This implied that the high particle-phase PAEs concentrations in summer resulted from enhanced emissions and stronger gas-particle conversion, and PAEs maintained relatively high levels in both the gas and particle phases during this season.

DEHP serves primarily as a plasticizer for polyvinyl chloride, accounting for approximately 80% of total PAEs production in China (Meng et al., 2014). DnBP is another extensively applied PAEs worldwide, and the consumption volumes of both compounds have undergone continuous rapid growth in recent decades (Gao and Wen, 2016). In this study, DnBP and DEHP were the predominant PAEs at NC in summer and winter, accounting for 62.9% and 41.0% of total PAEs, respectively; while DnBP was the predominant PAEs at YB, contributing 53.7% and 62.9% to total PAEs in summer and winter. These compositional variations imply distinct source compositions of PAEs between the two cities.

https://doi.org/10.5194/egusphere-2026-6761
Preprint. Discussion started: 11 November 2026
© Author(s) 2026. CC BY 4.0 License.

3.3 Diurnal variations of NPOCs

In summer, the four categories of NPOCs exhibited identical diurnal variations in the two cities (Fig. 5). Concentrations of n-alkanes, hopanes, and PAEs were higher during daytime than at night, which was likely related to higher temperatures and stronger source emissions in daytime. By contrast, nighttime PAHs concentrations in NC and YB were 1.8 and 1.9 times those in daytime, respectively. This can be explained by the fact that high daytime temperatures in summer drive portions of PAHs (especially LMW and MMW PAHs) into the gas phase, where they undergo rapid photooxidative degradation. At night, photodegradation is largely suppressed, and decreasing temperatures facilitate the partitioning of LMW and MMW PAHs from the gas phase to particle phase, leading to their accumulation.

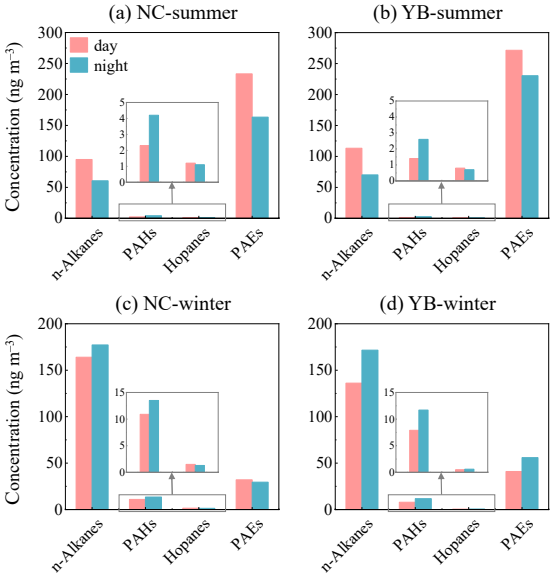


Figure 5: Diurnal concentration comparisons of four categories of NPOCs at NC and YB in summer and winter.

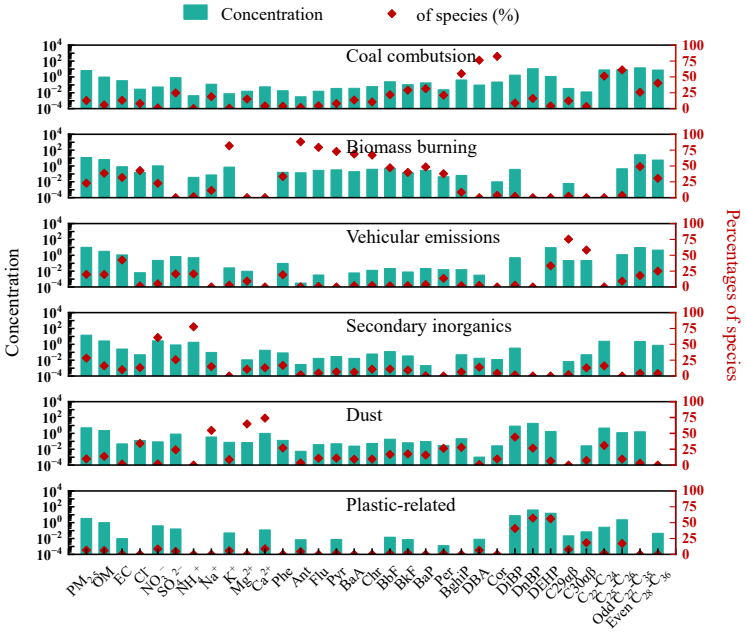
In winter, notable diurnal differences existed at both cities. At NC, concentrations of n-alkanes and PAHs were higher at night, while hopanes and PAEs showed higher levels in the daytime. At YB, all four categories of NPOCs species presented higher values during nighttime. Furthermore, at Chengdu, only PAEs had higher concentrations in the daytime, and the other three NPOCs showed higher values at night (Fig. S3). The spatial variations in diurnal characteristics are linked to their multiple sources and distinct source contributions at these cities.

3.4 Source apportionment of $PM_{2.5}$

Based on the PMF model, six sources were resolved for $PM_{2.5}$ at both NC and YB, namely coal combustion, biomass burning, vehicular emissions, secondary inorganic, dust, and plastic-related sources. Given the high consistency in factor

https://doi.org/10.5194/egusphere-2026-6761
Preprint. Discussion started: 11 November 2026
© Author(s) 2026. CC BY 4.0 License.

profiles of individual sources between the two cities, the $PM_{2.5}$ source profiles derived from NC were adopted as the representative case for analysis herein (Fig. 6), while the PMF factor profiles for YB are provided in the Fig. S4.



395

Figure 6: PMF source factor profiles for $PM_{2.5}$ at NC in terms of concentrations (μg m^{-3} for $PM_{2.5}$, carbonaceous species, and ions; ng m^{-3} for NPOCs) and percentages (%).

Factor 1 exhibited high loadings of Ca^{2+}, HMW PAHs (such as BbF, BkF, BaP, Bghip, DBA, and Cor), and LMW n-alkanes. HMW PAHs and LMW n-alkanes are well-established tracers of coal combustion (Li et al., 2025; Lin et al., 2011), and Ca^{2+} is a major component of fly ash generated during coal combustion (Guo et al., 2024; Tian et al., 2021). Accordingly, factor 1 was assigned to the coal combustion. Factor 2 exhibited high loadings of K^+, odd-carbon n-alkanes (C_{27}–C_{35}), and abundant PAHs such as Phe, Ant, Flu, Pyr, BaA, and Chr. The K^+ is a well-recognized tracer for biomass burning, and odd-carbon long-chain n-alkanes originate from plant epicuticular waxes. The co-occurrence of these markers together with abundant combustion-derived PAHs supports the assignment of this factor to the biomass burning (Guo et al., 2024; Haque et al., 2026). Factor 3 exhibited high loadings of $C_{29}\alpha\beta$ and $C_{30}\alpha\beta$ hopanes, which are widely accepted molecular tracers for vehicular emissions, originating from lubricating oil of motor vehicles (Cao et al., 2021; Guo et al., 2024). Thus, this factor was assigned to the vehicular emissions. Factor 4 exhibited high loadings of SO_4^{2-}, NO_3^-, and NH_4^+. These ions are typical secondary inorganic aerosol components formed via atmospheric oxidation and gas-to-particle conversion processes (Zhang et al., 2024a; Huang et al., 2017). Therefore, factor 4 was assigned to the secondary inorganic source. Factor 5 exhibited high loadings of Na^+, Mg^{2+}, and Ca^{2+}. These ions are typical crustal elements enriched in mineral particles (Zhang et al., 2024a;

https://doi.org/10.5194/egusphere-2026-6761
Preprint. Discussion started: 11 November 2026
© Author(s) 2026. CC BY 4.0 License.

Tian et al., 2021). Thus factor 5 was assigned to the dust source. Factor 6 exhibited high loadings of DiBP, DnBP, and DEHP. These three compounds are common PAEs widely used as plasticizers in plastic products. Accordingly, factor 6 was assigned to the plastic-related source.

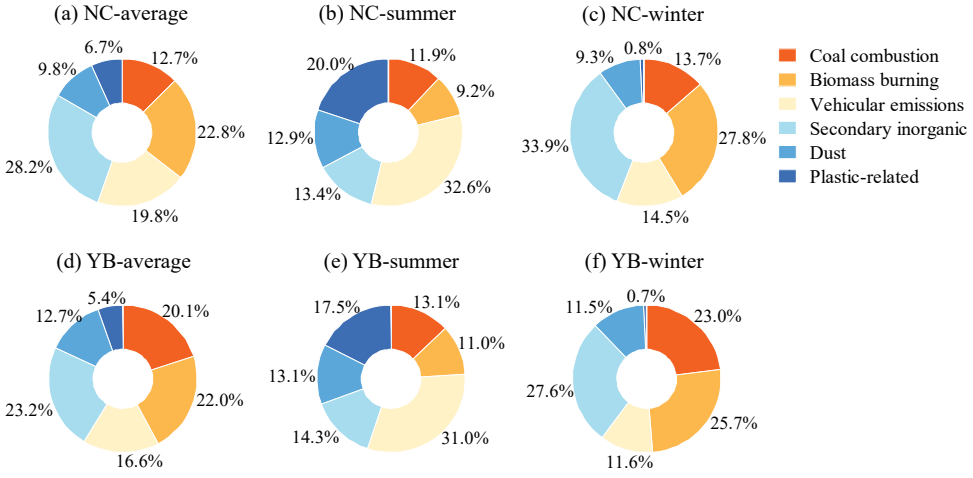


Figure 7: $PM_{2.5}$ source compositions of NC and YB for the (a, d) summer-winter averaged, (b, e) summer, and (c, f) winter periods.

As shown in Figs. 7a and d, secondary inorganic sources represented the largest fraction of summer-winter averaged $PM_{2.5}$ sources in both cities, with contributions of 28.2 % and 23.2 % at NC and YB, respectively. Meanwhile, discrepancies were also observed for other source between the two cities: NC exhibited higher contributions from biomass burning, vehicular emissions, and plastic-related sources, whereas YB showed higher contributions from coal combustion and dust.

All $PM_{2.5}$ sources exhibit similar seasonal variation patterns in both cities. Vehicular emissions dominate summer $PM_{2.5}$, reaching 32.6% at NC and 31.0% at YB, while their contributions decrease substantially in winter (14.5% and 11.6%, respectively). Dust contributions decline from 12.9% (NC) and 13.1% (YB) in summer to 9.3% and 11.5% in winter, largely due to weaker surface wind erosion in cold seasons. Plastic-related emissions drop sharply from 20.0% (NC) and 17.5% (YB) in summer to merely 0.8% and 0.7% in winter, as low temperatures suppress the release of volatile products from plastic waste. In contrast, biomass burning rises from 9.2% (NC) and 11.0% (YB) in summer to 27.8% and 25.7% in winter, linked to enhanced winter agricultural residue burning. Contributions from the other combustion source, coal combustion, increased from 11.9% (NC) and 13.1% (YB) to 13.7% and 23.0%, respectively. In addition, secondary inorganic sources also increased from 13.4% (NC) and 14.3% (YB) in summer to 33.9% and 27.6% in winter, favored by high humidity and stagnant conditions that accelerate secondary inorganic aerosol formation.

Compared with winter observations in Chengdu (Figs. S5 and S6), NC and YB exhibited higher contributions from biomass burning and secondary inorganic sources in winter. By contrast, Chengdu showed stronger contributions from vehicular

https://doi.org/10.5194/egusphere-2026-6761
Preprint. Discussion started: 11 November 2026
© Author(s) 2026. CC BY 4.0 License.

emissions, plastic-related, and dust sources. Meanwhile, compared with previous source apportionment results without NPOCs (Huang et al., 2017; Zhang et al., 2024a), the source apportionment incorporating NPOCs yields more comprehensive source information, such as plastic-related sources. The differences in contributions of such sources between medium-sized cities and the megacity further demonstrate the disparities in $PM_{2.5}$ sources across different types of cities.

3.5 NPOCs size-specific distributions in winter

Figure 8 presents the particle size distributions of NPOCs at the two cities during winter. It can be found that PAHs, hopanes, and n-alkanes were predominantly concentrated in fine particles (< 2.1 μm), and the concentration contribution of each species was below 10% across all size fractions larger than 2.1 μm. For individual NPOCs, the maximum concentrations of n-alkanes at NC and YB occurred in 0.65–1.1 μm and 1.1–2.1 μm, accounting for 24.5% and 20.6% of their total n-alkanes, respectively. Afterwards, n-alkane concentrations declined as particle size increased. This indicates that n-alkanes tend to adsorb onto fine particles. In general, condensation preferentially takes place on fine particles due to their large quantity and larger specific surface area (Wang et al., 2009). A similar size distribution pattern was also reported by Han et al. (2018), who found that n-alkanes were most abundant in the 0.56–1.00 μm particle fraction.

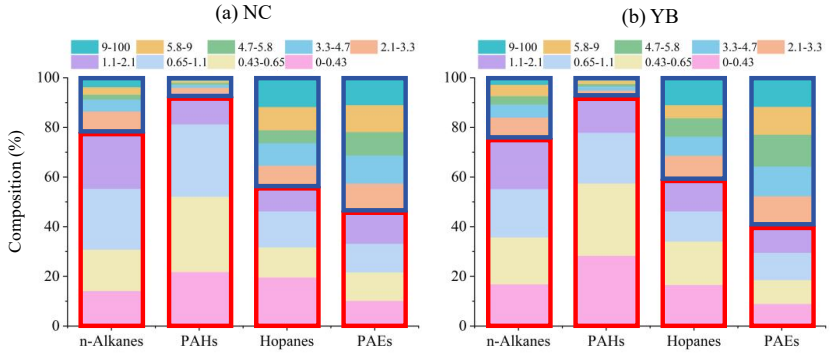


Figure 8: Relative composition of size distributions of four NPOC species at NC and YB in winter (particle size in μm; the red box denotes the total contribution for particle sizes smaller than 2.1 μm, the blue box represents the total contribution for particle sizes larger than 2.1 μm).

PAHs at both NC and YB reached their maximum concentrations in 0.43–0.65 μm, accounting for 30.3% and 29.1% of the total concentration, respectively. Such distribution characteristic can be well interpreted by previous observation that HMW PAHs are preferentially accumulated in fine particles below 1.4 μm (Kleeman et al., 2008). This enrichment pattern is mainly derived from gas-particle partitioning processes, including condensation partitioning of gaseous PAHs and coagulation of combustion-derived substances onto pre-existing particulate surfaces. In this study, the HMW PAHs accounted for 64.0% (NC) and 63.6% (YB) of the total PAHs, which confirmed our hypothesis that the condensation or coagulation of combustion products contributed to the size distribution pattern of PAHs. Similarly, Han et al. (2018) also

https://doi.org/10.5194/egusphere-2026-6761
Preprint. Discussion started: 11 November 2026
© Author(s) 2026. CC BY 4.0 License.

found that PAHs in the 0.56–1.00 μm fraction were the most abundant in urban aerosols of eastern China.

The peak size fraction of hopanes differed between the two cities: the maximum contribution of hopanes occurred at < 0.43 μm (19.7%) at NC and at 0.43–0.65 μm (17.5%) at YB, respectively. This ultrafine-mode size distribution pattern can be attributed to fossil fuel combustion. This finding is consistent with the work of Kleeman et al. (2008), who observed high hopane abundances in the ultrafine particle fraction during a severe winter pollution event in Sacramento, USA.

Distinct from the above three NPOC species, PAEs showed relatively uniform contributions across all nine particle size fractions, with mass percentages ranging from 9.5% to 13.0% at NC and from 9.0% to 12.8% at YB, respectively. Notably, PAEs had higher proportions in coarse particles (> 2.1 μm), which accounted for 53.7% and 59.8% of the total in NC and YB, respectively. This distinct distribution pattern demonstrates that PAEs differ substantially from other NPOCs in terms of emission origins and atmospheric partitioning behaviors: (1) The other NPOCs are predominantly combustion-derived pollutants, which are primarily emitted as fine-mode particulates. Their strong hydrophobicity, coupled with the large specific surface area of fine particles, facilitates their preferential accumulation in fine particle fractions. In comparison, PAEs mainly stem from microplastic debris and plasticizer residuals, contaminants intrinsically characterized by coarse particle sizes during primary emission; (2) Furthermore, PAEs are typical semi-volatile organic compounds that readily form organic films on particulate surfaces. The continuous and intact organic coatings on coarse particles can greatly promote the hydrophobic partitioning of PAEs, ultimately resulting in the predominant enrichment of PAEs in coarse particle fractions.

3.6 Health risk and source attribution associated with PAHs

3.6.1 BaP_{eq} and LLCR

Our calculations revealed that the BaP_{eq} of NC were 0.4 ng m^{-3} in summer and 1.7 ng m^{-3} in winter, respectively, while those of YB were 0.3 ng m^{-3} and 1.2 ng m^{-3}, respectively. These are markedly lower than those documented for several typical regions of China, including the Yangtze River Delta (i.e., 3.86 ± 1.00 ng m^{-3} in Nanjing) (Cao et al., 2021), northern Chinese (i.e., 5.58 ± 1.63 ng m^{-3} in Beijing), northwest China (i.e., 17.16 ± 8.68 ng m^{-3} in Xi'an), and central China (i.e., 7.12 ± 2.38 in Wuhan) (Sun et al., 2022). In addition, the calculated BaP_{eq} value for Chengdu (1.7 ng m^{-3}) in winter 2023 is nearly identical to that of NC in winter and slightly higher than the winter value of YB.

The LLCR values for NC were 0.3×10^{-4} in summer and 1.5×10^{-4} in winter, while the corresponding values for YB were 0.2×10^{-4} and 1.0×10^{-4}, respectively. The USEPA categorized the cancer risks into five levels: very low (LLCR < 10^{-6}), low ($10^{-6} \leq$ LLCR < 10^{-4}), moderate ($10^{-4} \leq$ LLCR < 10^{-3}), high ($10^{-3} \leq$ LLCR < 10^{-1}), and very high (LLCR > 10^{-1}) (Zhang et al., 2019). Accordingly, the health risk induced by exposure to $PM_{2.5}$-bound PAHs was at a low level in summer for both cities, whereas it fell into the moderate risk category in winter. The seasonal patterns of LLCR risk levels are consistent with

https://doi.org/10.5194/egusphere-2026-6761
Preprint. Discussion started: 11 November 2026
© Author(s) 2026. CC BY 4.0 License.

those reported in Hangzhou, albeit with numerical discrepancies (0.08×10^{-4} in summer and 2.99×10^{-4} in winter). Furthermore, the LLCR values are lower than field-measured results from several cities in central China, exemplified by an annual mean LLCR of 3.03×10^{-4} in Wuhan (Zhang et al., 2019).

3.6.2 Sources of LLCR

Source apportionment of LLCR in the two cities was conducted using the PMF model. Finally, four major sources were resolved, namely coal combustion, vehicular emissions, industrial emissions, and biomass burning. The profiles of PMF factors for NC and YB are shown in Figs S7 and S8, and the source composition for different periods is illustrated in Fig. 9.

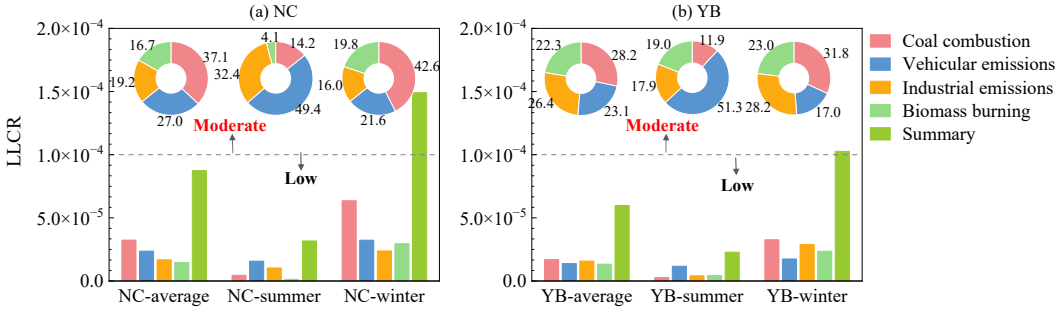


Figure 9: Source composition of PAH-related LLCR at NC and YB in summer and winter.

As shown in Fig. 9, coal combustion was the dominant source of seasonally averaged LLCR at NC, with a contribution of 37.1%, followed by vehicular emissions (27.0%). Industrial emissions and biomass burning contributed less than 20% (at 19.2% and 16.7%). Coal combustion was also the largest contributor to seasonally averaged LLCR at YB. Unlike NC, the four sources at YB exhibited relatively small differences in their contributions, ranging from 22.3% to 28.2%.

LLCR sources in both cities showed pronounced seasonal variations. Vehicular emissions dominated LLCR sources in NC during summer, contributing 49.4% of total LLCR, followed by industrial sources (32.4%) and coal combustion (14.2%); biomass burning contributed the smallest fraction (4.1%). In winter, however, contributions from the two combustion sources (i.e., coal combustion and biomass burning) increased substantially. Coal combustion became the predominant LLCR source with a contribution of 42.6%, while biomass burning contributed 19.8%. In contrast, the contributions of vehicular and industrial emissions decreased markedly relative to summer, at 21.6% and 16.0%, respectively (Fig. 9a).

Similar to the summer scenario at NC, vehicular emissions remained the dominant source of LLCR at YB during summer, with a contribution rate of 51.3%. Biomass burning constituted the second largest source (19.0%). This value was substantially higher than the summer level of 4.1% in NC, highlighting the critical contribution of biomass burning to PAHs-related LLCR at YB. In addition, industrial sources and coal combustion contributed 17.9% and 11.9% to the summer

https://doi.org/10.5194/egusphere-2026-6761
Preprint. Discussion started: 11 November 2026
© Author(s) 2026. CC BY 4.0 License.

LLCR at YB, respectively (Fig. 9b). Consistent with the seasonal variations observed in NC, the contribution of coal combustion at YB increased drastically in winter, reaching 31.8% and becoming the dominant source. In contrast, the contribution of vehicular emissions dropped sharply to merely 17.0%. Furthermore, industrial emissions and biomass burning contributed 28.2% and 23.0% to the winter LLCR at YB, respectively.

Chengdu exhibited a distinct LLCR source profile in winter compared with the two medium-sized cities (Fig. S10). Vehicular emissions dominated with the highest contribution of 35.8 %, highlighting the substantial influence of over 8 million motor vehicles on LLCR in this megacity. In contrast, contributions from coal combustion and biomass burning were considerably lower in Chengdu (25.2 % and 11.0 %, respectively) than in the two medium-sized cities. This is largely attributable to stricter emission controls on these two combustion sources in Chengdu: primary emissions of these pollutants are nearly absent within the urban area, and they are mostly derived from long-range transport from surrounding regions.

Overall, vehicular emissions were the primary source of PAHs-related LLCR in summer in the two medium-sized cities. While in winter, the contributions of combustion sources (coal combustion and biomass burning) increased markedly. Notably, coal combustion emerged as the predominant common source of PAHs-related LLCR in the two medium-sized cities. Moreover, driven by the large fleet of motor vehicles, vehicular emissions was the dominant contributor to LLCR in Chengdu even during winter.

3.7 Evolution of NPOCs with pollution

According to the Technical Specifications on Ambient Air Quality Index (AQI, HJ 633-2026), the four observation periods in this study can be further categorized by air quality, such as non-polluted (NP) days ($0 < AQI < 100$), lightly polluted (LP) days ($100 < AQI < 150$), and moderately polluted (MP) days ($150 < AQI < 200$). As shown in Figure S11, no polluted days were observed during the summer campaign at NC, and all days were classified as NP days. In contrast, the summer campaign at YB comprised both NP and LP days. In winter, air pollution levels at both sites increased significantly, with NP, LP, and MP days all captured. To gain deeper insights into NPOCs, this section further explores the evolutionary characteristics of NPOCs across days with different air quality levels. The summer campaign at NC was excluded from this discussion because no polluted days were observed.

3.7.1 NPOCs mass concentration and composition

In YB summer, the total concentration of NPOCs increased from 317.8 ± 110.2 ng m^{-3} on NP to 521.4 ± 211.8 ng m^{-3} on LP days. The concentrations of the four types of NPOCs all increased to varying degrees. Specifically, the relative increment of n-alkanes reached 151.2% (from 76.1 ± 35.0 ng m^{-3} to 191.3 ± 219.9 ng m^{-3}), which was substantially higher than the 34.3%–40.7% increments of the other three NPOCs, indicating that n-alkanes contributed dominantly to the elevation of

https://doi.org/10.5194/egusphere-2026-6761
Preprint. Discussion started: 11 November 2026
© Author(s) 2026. CC BY 4.0 License.

total NPOCs concentrations during pollution aggravation. In terms of relative contribution (Fig. 10a), the proportion of n-alkanes rose from 23.2% to 31.6%. We also found that although the HMW/LMW ratio increased from 2.0 to 3.5 during pollution accumulation, this variation did not suggest an elevated contribution from natural sources. This can be evidenced by the following observations. First, the CPI of n-alkanes decreased from 1.5 to 1.4, indicating that enhanced anthropogenic emissions. Second, the WNA% dropped from 20.0% to 12.6%, which means the contribution of anthropogenic n-alkanes increased from 80.0% to 87.4%. Third, the correlation coefficient R^2 between n-alkanes and levoglucosan increased from 0.20 to 0.35, which implies that biomass burning likely played a more important role in elevating the concentrations and contributions of n-alkanes. Unlike n-alkanes, PAHs and hopanes exhibited nearly stable contributions, while the contributions of PAEs declined.

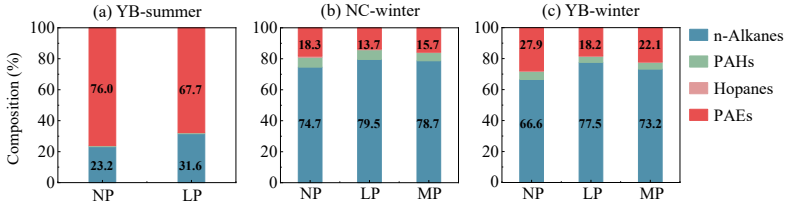


Figure 10: Chemical composition of NPOCs at NC and YB under different pollution levels.

During winter in NC, the total NPOCs concentration increased from 175.4 ± 115.3 ng m^{-3} to 365.8 ± 126.1 ng m^{-3} from NP to MP days. Except for hopanes, which decreased by 0.4 ng m^{-3}, the concentrations of the other three NPOCs increased substantially, among which n-alkanes showed the largest increment of 148.1 ng m^{-3}. The NPOCs composition also varied with pollution aggravation: the contribution of n-alkanes rose from 74.7% to 78.7%, while the contributions of the other three NPOCs decreased by 0.4%–2.6% (Fig. 10b). Winter YB exhibited a highly consistent variation trend with winter NC (Fig. 10c). From NP to MP days, the NPOCs concentration increased from 152.5 ± 96.9 ng m^{-3} to 349.9 ± 92.3 ng m^{-3}. Similarly, all NPOCs increased obviously except hopanes, which only rose slightly by 0.3 ng m^{-3}, and n-alkanes presented a prominent increment of 156.0 ng m^{-3}. In addition, the contribution of n-alkanes increased by 6.6% from NP to MP days, whereas the contributions of the other three NPOCs declined to varying degrees (0.1%–5.8%). These results indicate that n-alkanes play a critical role in driving the elevation of NPOCs concentrations during winter pollution aggravation in the two medium-sized cities.

Compared with winter in the two medium-sized cities, Chengdu exhibited higher NPOCs concentrations across all pollution levels during winter. From NP to MP days, the total NPOCs concentration increased from 508.4 ± 218.2 ng m^{-3} to 894.2 ± 209.7 ng m^{-3}. PAEs remained the dominant NPOCs, although their contribution decreased slightly by 1.1% as pollution worsened (Fig. S12). Furthermore, from NP to MP days, the contribution of n-alkanes increased by 1.6%, while the

https://doi.org/10.5194/egusphere-2026-6761
Preprint. Discussion started: 11 November 2026
© Author(s) 2026. CC BY 4.0 License.

contributions of the other two NPOCs remained relatively low, varying in the ranges of 1.6%-2.1% and 0.17%-0.19%, respectively.

3.7.2 $PM_{2.5}$ sources composition

In YB summer, from NP to LP days the contributions of vehicular emissions, secondary inorganic sources, and dust increased by 5.3%, 1.5%, and 2.3%, respectively, whereas coal combustion, biomass burning, and plastic-related sources decreased by 3.7%, 2.3%, and 3.2% (Fig. 11a). This indicates that the formation of summer pollution in YB is jointly driven by local emissions, such as urban vehicle and dust, as well as the formation of secondary pollution.

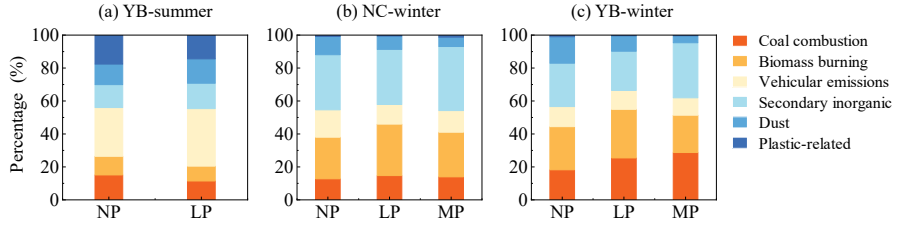


Figure 11: Evolution of $PM_{2.5}$ source compositions with pollution severity at NC and YB.

In winter at NC, the contributions of coal combustion and biomass burning both showed a trend of first increasing and then decreasing from NP to MP days, with their maximum contributions occurring on LP days (14.7% and 31.3%, respectively) (Fig. 11b). Vehicular emissions exhibited an opposite trend, i.e., first decreasing and then increasing. In addition, the contribution of secondary inorganic sources remained stable at 33.5% on both NP and LP days, and rose by 5.4% during the evolution from LP to MP days. By contrast, the contribution of dust sources decreased continuously, with a total reduction of 5.3%. Therefore, during winter haze episodes at NC, coal combustion and biomass burning jointly facilitated the formation of LP days, while vehicular emissions and secondary inorganic sources were the key $PM_{2.5}$ sources driving the further deterioration of pollution from LP to MP days.

In winter at YB, coal combustion was the only source with a continuously increasing contribution from NP to MP days, with an increment of 10.5%, making it the dominant contributor to pollution aggravation (Fig. 11c). Meanwhile, biomass burning and secondary inorganic sources played important roles in the pollution evolution during the NP-to-LP and LP-to-MP days, with corresponding increases of 3.3% and 9.6%, respectively. Moreover, the contributions of vehicular emissions, dust, and plastic-related sources all decreased continuously.

Wintertime Chengdu exhibited a different scenario from these two medium-sized cities (Fig. S13). As pollution worsened, contributions from coal combustion and vehicular emissions both rose first and then declined substantially, with their maximum contributions occurring on LP days and minimum contributions on MP days. Meanwhile, contributions from

https://doi.org/10.5194/egusphere-2026-6761
Preprint. Discussion started: 11 November 2026
© Author(s) 2026. CC BY 4.0 License.

biomass burning and dust sources decreased continuously, whereas the contribution of secondary inorganic sources increased markedly from 10.7% on NP to 48.9% on MP days. This indicates that coal combustion and vehicular emissions were the two dominant contributors to formation LP days. As pollution further intensified, however, their contributions diminished, while secondary inorganic sources persisted throughout the whole pollution buildup process, accounting for nearly half of the total $PM_{2.5}$ on MP days. These results imply that pollution mitigation strategies for different city types and seasons within the SCB should target distinct primary sources.

3.7.3 NPOCs size distribution

As shown in Fig. 12, NPOCs exhibited marked differences in particle size distributions with increasing winter air pollution in the two cities. In NC winter, all NPOC species, except hopanes, exhibited an evident shift of peak concentration fractions from fine to coarse particles from NP to P (including LP and MP) days. Specifically, on NP days, n-alkanes, PAHs, and PAEs peaked at the particle size ranges of 0.65–1.1 μm (26.8%), 0.43–0.65 μm (35.2%), and 0.43–0.65 μm (13.5%), respectively. Their peak fractions shifted to coarser ranges of 1.1–2.1 μm (25.7%), 0.65–1.1 μm (29.4%), and 1.1–2.1 μm (13.6%) on P days, whereas the peak fraction of hopanes remained stable at <0.43 μm under both NP and P days. Moreover, the cumulative mass contributions of all NPOCs, except hopanes, in the submicron particle size range (< 1.1 μm) decreased as pollution worsened, which strongly demonstrates the universal coarsening trend of the NPOCs particle size on P days. This is mainly because during P days, high particle concentration and stagnant meteorological conditions promote frequent collision, coagulation, and hygroscopic growth of fine particles. Gaseous NPOCs tends to adsorb onto coarse particles, and newly formed secondary organic aerosols also attach to larger particles. These processes collectively lead to the reduction of NPOCs mass contribution in the submicron range and the overall particle coarsening.

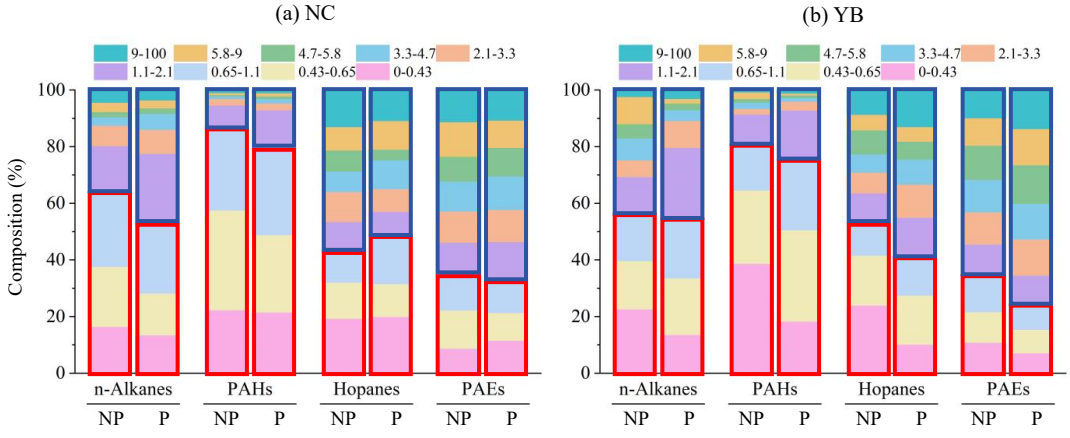


Figure 12: Relative composition of size-resolved NPOC species at NC and YB during non-polluted (NP) and polluted (P) days

https://doi.org/10.5194/egusphere-2026-6761
Preprint. Discussion started: 11 November 2026
© Author(s) 2026. CC BY 4.0 License.

(particle size in μm; the red box denotes the total contribution for particle sizes smaller than 1.1 μm, the blue box represents the total contribution for particle sizes larger than 1.1 μm).

In YB winter, all NPOCs also presented a distinct particle size coarsening phenomenon under aggravated pollution conditions. From NP to P days, the peak particle size fractions of n-alkanes, PAHs, hopanes, and PAEs shifted from <0.43 μm (22.6%), <0.43 μm (38.7%), <0.43 μm (23.9%), and 0.65–1.1 μm (13.1%) to 1.1–2.1 μm (24.5%), 0.43–0.65 μm (32.2%), 0.43–0.65 μm (17.3%), and 4.7–5.8 μm (13.7%), respectively. Similarly, all NPOCs showed significant reductions in their cumulative proportions in the submicron particle size range on P days.

4 Summary and implications

NPOCs constitute an important chemical component of organic aerosols. To gain a comprehensive understanding of atmospheric NPOCs in the SCB, one of the most severely haze-affected regions in China, this study measured NPOCs in atmospheric particulate matter at two medium-sized cities (NC and YB) during summer and winter. We found that $PM_{2.5}$ concentrations at both cities were higher in winter than in summer, with winter levels being 3.4 and 3.5 times the summer values for NC and YB, respectively. A north-to-south gradual aggravation of $PM_{2.5}$ pollution was also observed across the SCB. Forty-eight NPOCs were identified. Their summer concentrations were 1.3 (NC) and 1.6 (YB) times their winter counterparts. The detected NPOCs were classified into four groups: n-alkanes, PAHs, hopanes, and PAEs. Driven by high summer temperatures, PAEs represented the most abundant compound class in summer, accounting for 71.2%–74.9% of total NPOCs. In winter, anthropogenic contributions increased substantially, and n-alkanes prevailed, comprising 69.6%–76.5% of total NPOCs. PMF source apportionment, integrating carbonaceous components, water-soluble ions, and representative NPOC tracers, revealed that vehicular emissions were the dominant $PM_{2.5}$ source in summer for both cities, contributing 32.6% (NC) and 31.0% (YB), respectively, accompanied by considerable plastic-related contributions (20.0% and 17.5%). In winter, contributions from secondary inorganics and combustion sources both increased. Size-distribution measurements of winter NPOCs showed that PAHs, hopanes, and n-alkanes mainly accumulated in fine particles, whereas PAEs were more abundant in coarse particles. $PM_{2.5}$-bound PAHs exerted low health risks in summer and moderate risks in winter. Vehicular emissions contributed nearly half of summer LLCR, whereas coal combustion and biomass burning dominated winter LLCR. Pollution-evolution analyses for YB in summer and for both cities in winter indicated that PAEs prevailed alongside rising n-alkanes as pollution deteriorated in YB summer, while n-alkanes became more dominant under winter conditions. Vehicular emissions exhibited the largest growth during summer pollution in YB, whereas winter pollution in both cities was driven by combustion and secondary inorganic sources. With the exception of hopanes at NC, all NPOC species displayed particle-size coarsening as pollution intensified in winter.

https://doi.org/10.5194/egusphere-2026-6761
Preprint. Discussion started: 11 November 2026
© Author(s) 2026. CC BY 4.0 License.

To obtain a more comprehensive understanding of NPOCs across the SCB and to explore discrepancies between medium-sized cities and megacities, we compared observations from the two medium-sized cities in this study with winter measurements collected in Chengdu in 2023 (Zhang et al., 2025). Distinct differences in NPOCs were identified among different city types in the SCB. First, in terms of chemical composition, winter NPOCs in Chengdu were dominated by PAEs, with a contribution of 77.9%, which was substantially higher than the corresponding values of 16.7% and 25.2% at NC and YB. Second, compared with the medium-sized cities, winter $PM_{2.5}$ source contributions from vehicular emissions and plastic-related sources were higher in Chengdu, which is directly linked to its larger vehicle fleet and abundant plastic-related emission sources. Meanwhile, owing to more stringent control measures, contributions from combustion sources in Chengdu were lower than those in the medium-sized cities. Source apportionment of LLCR also revealed the predominant roles of vehicular emissions in the megacity and combustion sources in the medium-sized cities, respectively. Pollution evolution in Chengdu exhibited greater complexity: coal combustion and vehicular emissions acted as the two major contributors to $PM_{2.5}$ formation on LP days. Nevertheless, their contributions declined as pollution further aggravated, whereas secondary inorganic sources persisted throughout the entire pollution-build-up period and accounted for nearly half of total $PM_{2.5}$ on MP days.

In addition, it is noteworthy that this study reveals that the contribution of vehicular emissions to LLCR exceeds its contribution to $PM_{2.5}$ mass concentration across all observation periods, which directly highlights the significance of this emission source for atmospheric pollution-related health research. This finding agrees well with previous reports showing that traffic-derived particulate matter accounts for only 14.7% of total $PM_{2.5}$ mass but contributes to 73.6% of $PM_{2.5}$-attributable cancer deaths (Yu et al., 2026). Over the past decade, China has witnessed a rapid rise in vehicle ownership, reaching 469 million by 2025. Within the SCB, Chengdu recorded a vehicle ownership of 8.2 million at the end of 2025. The vehicle numbers in NC and YB exceeded 1.3 million and 1.1 million, respectively, and are still growing rapidly. This implies that traffic-related sources deserve special attention in future health risk studies of atmospheric pollution over the SCB region.

Data availability.

The data used in this work can be found at https://doi.org/10.5281/zenodo.23800734 (Zhang et al., 2026).

Author contributions.

JZ and GW planned this campaign; JZ wrote the paper and led this research; YZ performed the data analysis and wrote the manuscript together with JZ; YZ, XY, WZ, SL, YC, and KS conducted experiments and instrument maintenance; XY and

https://doi.org/10.5194/egusphere-2026-6761
Preprint. Discussion started: 11 November 2026
© Author(s) 2026. CC BY 4.0 License.



WZ helped with the data analysis. GW made comprehensive revisions and comments on the manuscript. All authors approved the final version of the manuscript.

Competing interests.

The authors declare that they have no conflict of interest.

Financial support.

This research has been supported by the National Natural Science Foundation of China (grant nos. 22676196 and U23A2030).

References

Bootdee, S., Chantara, S., and Prapamontol, T.: Determination of $PM_{2.5}$ and polycyclic aromatic hydrocarbons from incense burning emission at shrine for health risk assessment, Atmos. Pollut. Res., 7, 680–689, https://doi.org/10.1016/j.apr.2016.03.002, 2016.

Cao, F., Zhang, Y. X., Lin, X., and Zhang, Y. L.: Characteristics and source apportionment of non-polar organic compounds in $PM_{2.5}$ from the three megacities in Yangtze River Delta region, China, Atmos. Res., 252, 105443, https://doi.org/10.1016/j.atmosres.2020.105443, 2021.

Cheng, Y. F., Zheng, G. J., Wei, C., Mu, Q., Zheng, B., Wang, Z. B., Gao, G., Zhang, Q., He, K. B., Carmichael, G., Pöschl, U., and Su, H.: Reactive nitrogen chemistry in aerosol water as a source of sulfate during haze events in China, Sci. Adv., 2, e1601530, https://doi.org/10.1126/sciadv.1601530, 2016.

Chow, J. C., Watson, J. G., Chen, L. W., Chang, M. C., Robinson, N. F., Trimble, D., and Kohl, S.: The IMPROVE_A temperature protocol for thermal/optical carbon analysis: maintaining consistency with a long-term database, J. Air Waste Manage., 57, 1014–1023, https://doi.org/10.3155/1047-3289.57.9.1014, 2007.

Ding, X., Wang, X., Xie, Z., Xiang, C., Mai, B., Sun, L., Zheng, M., Sheng, G., Fu, J., and Pöschl, U.: Atmospheric polycyclic aromatic hydrocarbons observed over the North Pacific Ocean and the Arctic area: Spatial distribution and source identification, Atmos. Environ., 41, 2061–2072, https://doi.org/10.1016/j.atmosenv.2006.11.002, 2007.

Duan, L., Yu, H., Wang, Q., Cao, Y., Wang, G., Sun, X., Li, H., Lin, T., and Guo, Z.: $PM_{2.5}$-bound polycyclic aromatic hydrocarbons of a megacity in eastern China: Source apportionment and cancer risk assessment, Sci. Total Environ., 869, 161792, https://doi.org/10.1016/j.scitotenv.2023.161792, 2023.

https://doi.org/10.5194/egusphere-2026-6761
Preprint. Discussion started: 11 November 2026
© Author(s) 2026. CC BY 4.0 License.



Fan, Y., Liu, C., Li, L., Ren, L., Ren, H., Zhang, Z., Li, Q., Wang, S., Hu, W., Deng, J., Wu, L., Zhong, S., Zhao, Y., Pavuluri, C. M., Li, X., Pan, X., Sun, Y., Wang, Z., Kawamura, K., Shi, Z., and Fu, P.: Large contributions of biogenic and anthropogenic sources to fine organic aerosols in Tianjin, North China, Atmos. Chem. Phys., 20, 117–137, https://doi.org/10.5194/acp-20-117-2020, 2020.

Farah, E., Fadel, M., Mansour, G., Fakhri, N., Hassan, S. K., Boraiy, M., El-Nazer, M., Wheida, A., Abdelwahab, M., Oikonomou, K., Sauvage, S., Borbon, A., Sciare, J., Courcot, D., Ledoux, F., and Afif, C.: Unveiling the organic chemical composition and sources of organic carbon in $PM_{2.5}$ at an urban site in Greater Cairo (Egypt): A comprehensive analysis of primary and secondary compounds, Environ. Res., 263, 120118, https://doi.org/10.1016/j.envres.2024.120118, 2024.

Fu, P., Kawamura, K., and Miura, K.: Molecular characterization of marine organic aerosols collected during a round-the-world cruise, J. Geophys. Res.-Atmos., 116, D015604, https://doi.org/10.1029/2011jd015604, 2011.

Fu, P., Kawamura, K., Okuzawa, K., Aggarwal, S. G., Wang, G., Kanaya, Y., and Wang, Z.: Organic molecular compositions and temporal variations of summertime mountain aerosols over Mt. Tai, North China Plain, J. Geophys. Res.-Atmos., 113, D009900, https://doi.org/10.1029/2008jd009900, 2008.

Fu, P. Q., Kawamura, K., Pavuluri, C. M., Swaminathan, T., and Chen, J.: Molecular characterization of urban organic aerosol in tropical India: contributions of primary emissions and secondary photooxidation, Atmos. Chem. Phys., 10, 2663–2689, https://doi.org/10.5194/acp-10-2663-2010, 2010.

Fu, P. Q., Kawamura, K., Chen, J., Li, J., Sun, Y. L., Liu, Y., Tachibana, E., Aggarwal, S. G., Okuzawa, K., Tanimoto, H., Kanaya, Y., and Wang, Z. F.: Diurnal variations of organic molecular tracers and stable carbon isotopic composition in atmospheric aerosols over Mt. Tai in the North China Plain: an influence of biomass burning, Atmos. Chem. Phys., 12, 8359–8375, https://doi.org/10.5194/acp-12-8359-2012, 2012.

Gao, D. and Wen, Z.: Phthalate esters in the environment: A critical review of their occurrence, biodegradation, and removal during wastewater treatment processes, Sci. Total Environ., 541, 986–1001, https://doi.org/10.1016/j.scitotenv.2015.09.148, 2016.

Guo, W., Li, Z., Zhang, Z., Zhu, R., Xiao, H., and Xiao, H.: Sources and influences of atmospheric nonpolar organic compounds in Nanchang, central China: Full-year monitoring with a focus on winter pollution episodes, Sci. Total Environ., 912, 169216, https://doi.org/10.1016/j.scitotenv.2023.169216, 2024.

Han, D., Fu, Q., Gao, S., Li, L., Ma, Y., Qiao, L., Xu, H., Liang, S., Cheng, P., Chen, X., Zhou, Y., Yu, J. Z., and Cheng, J.: Non-polar organic compounds in autumn and winter aerosols in a typical city of eastern China: size distribution and impact of gas-particle partitioning on $PM_{2.5}$ source apportionment, Atmos. Chem. Phys., 18, 9375–9391, https://doi.org/10.5194/acp-18-9375-2018, 2018.

https://doi.org/10.5194/egusphere-2026-6761
Preprint. Discussion started: 11 November 2026
© Author(s) 2026. CC BY 4.0 License.



Haque, M. M., Boreddy, S. K. R., Jung, J., and Kawamura, K.: Source apportionment and health risk assessment of PM_{10}-bound organic aerosols in urban South Korea: Insights from n-alkanes, PAHs, hopanes, and steranes, Atmos. Res., 335, 108791, https://doi.org/10.1016/j.atmosres.2026.108791, 2026.

Haque, M. M., Kawamura, K., Deshmukh, D. K., Fang, C., Song, W., Mengying, B., and Zhang, Y. L.: Characterization of organic aerosols from a Chinese megacity during winter: predominance of fossil fuel combustion, Atmos. Chem. Phys., 19, 5147–5164, https://doi.org/10.5194/acp-19-5147-2019, 2019.

Huang, X., Tang, G., Zhang, J., Liu, B., Liu, C., Zhang, J., Cong, L., Cheng, M., Yan, G., Gao, W., Wang, Y., and Wang, Y.: Characteristics of $PM_{2.5}$ pollution in Beijing after the improvement of air quality, J. Environ. Sci., 100, 1–10, https://doi.org/10.1016/j.jes.2020.06.004, 2021.

Huang, X., Liu, Z., Ge, Y., Li, Q., Wang, X., Fu, H., Zhu, J., Zhou, B., Wang, L., George, C., Wang, Y., Wang, X., Su, J., Xue, L., Yu, S., Mellouki, A., and Chen, J.: Aerosol high water contents favor sulfate and secondary organic aerosol formation from fossil fuel combustion emissions, npj Clim. Atmos. Sci., 6, 504, https://doi.org/10.1038/s41612-023-00504-1, 2023.

Huang, X. J., Liu, Z. R., Liu, J. Y., Hu, B., Wen, T. X., Tang, G. Q., Zhang, J. K., Wu, F. K., Ji, D. S., Wang, L. L., and Wang, Y. S.: Chemical characterization and source identification of $PM_{2.5}$ at multiple sites in the Beijing–Tianjin–Hebei region, China, Atmos. Chem. Phys., 17, 12941–12962, https://doi.org/10.5194/acp-17-12941-2017, 2017.

IPCC: Climate Change 2023: Synthesis Report. Contribution of Working Groups I, II and III to the Sixth Assessment Report of the Intergovernmental Panel on Climate Change, edited by Core Writing Team, Lee, H. and Romero, J., IPCC, Geneva, Switzerland, https://doi.org/10.59327/IPCC/AR6-9789291691647, 2023.

Jia, Y. L., Stone, D., Wang, W. T., Schrlau, J., Tao, S., and Simonich, S. L. M.: Estimated reduction in cancer risk due to PAH exposures if source control measures during the 2008 Beijing Olympics were sustained, Environ. Health Persp., 119, 815–820, https://doi.org/10.1289/ehp.1003100, 2011.

Kang, M., Ren, L., Ren, H., Zhao, Y., Kawamura, K., Zhang, H., Wei, L., Sun, Y., Wang, Z., and Fu, P.: Primary biogenic and anthropogenic sources of organic aerosols in Beijing, China: Insights from saccharides and n-alkanes, Environ. Pollut., 243, 1579–1587, https://doi.org/10.1016/j.envpol.2018.09.118, 2018.

Kleeman, M. J., Riddle, S. G., and Jakober, C. A.: Size distribution of particle-phase molecular markers during a severe winter pollution episode, Environ. Sci. Technol., 42, 6469–6475, https://doi.org/10.1021/es800346k, 2008.

Li, L. J., Ho, S. S. H., Feng, B., Xu, H., Wang, T., Wu, R., Huang, W., Qu, L., Wang, Q., and Cao, J.: Characterization of particulate-bound polycyclic aromatic compounds (PACs) and their oxidations in heavy polluted atmosphere: A case study in urban Beijing, China during haze events, Sci. Total Environ., 660, 1392–1402,

https://doi.org/10.5194/egusphere-2026-6761
Preprint. Discussion started: 11 November 2026
© Author(s) 2026. CC BY 4.0 License.



https://doi.org/10.1016/j.scitotenv.2019.01.078, 2019.

Li, N., Li, Q., Zhu, F., Liu, P., Wang, Z., Chen, Z., Han, W., Wang, K., Hou, K., and Xu, Y.: Polycyclic aromatic hydrocarbons in road dust in Changchun City, Northeast China: spatial distribution, source appointment, and human health risk assessment, Adv. Meteorol., 2025, 8634494, https://doi.org/10.1155/adme/8634494, 2025.

Li, Y., Ren, H., Zhou, S., Pei, C., Gao, M., Liang, Y., Ye, D., Sun, X., Li, F., Zhao, J., Hang, J., Fan, S., and Fu, P.: Tower-based profiles of wintertime secondary organic aerosols in the urban boundary layer over Guangzhou, Sci. Total Environ., 950, 175326, https://doi.org/10.1016/j.scitotenv.2024.175326, 2024.

Liang, B., Su, Z., Tian, M., Yang, F., Gao, M., Chen, Y., Zhang, L., and Xiang, L.: Sources and potential health risks of $PM_{2.5}$-bound PAHs in a megacity of Southwest China: Importance of studying from a health risk perspective, Polycycl. Aromat. Comp., 42, 815–832, https://doi.org/10.1080/10406638.2020.1753218, 2020.

Lin, P., Aiona, P. K., Li, Y., Shiraiwa, M., Laskin, J., Nizkorodov, S. A., and Laskin, A.: Molecular characterization of brown carbon in biomass burning aerosol particles, Environ. Sci. Technol., 50, 11815–11824, https://doi.org/10.1021/acs.est.6b03024, 2016.

Lin, T., Hu, L., Guo, Z., Qin, Y., Yang, Z., Zhang, G., and Zheng, M.: Sources of polycyclic aromatic hydrocarbons to sediments of the Bohai and Yellow Seas in East Asia, J. Geophys. Res-Atmos., 116, D23305, https://doi.org/10.1029/2011JD015722, 2011.

Luo, J., Huang, X., Zhang, J., Luo, B., Zhang, W., and Song, H.: Characterization of aerosol particles during the most polluted season (winter) in urban Chengdu (China) by single-particle analysis, Environ. Sci. Pollut. R., 26, 17685–17695, https://doi.org/10.1007/s11356-019-05156-4, 2019.

Luo, J., Zhang, J., Huang, X., Liu, Q., Luo, B., Zhang, W., Rao, Z., and Yu, Y.: Characteristics, evolution, and regional differences of biomass burning particles in the Sichuan Basin, China, J. Environ. Sci., 89, 35–46, https://doi.org/10.1016/j.jes.2019.09.015, 2020.

Meng, X., Wang, Y., Xiang, N., Chen, L., Liu, Z., Wu, B., Dai, X., Zhang, Y., Xie, Z., and Ebinghaus, R.: Flow of sewage sludge-borne phthalate esters (PAEs) from human release to human intake: Implication for risk assessment of sludge applied to soil, Sci. Total Environ., 476–477, 242-249, https://doi.org/10.1016/j.scitotenv.2014.01.007, 2014.

Nisbet, I. C. T. and Lagoy, P. K.: Toxic equivalency factors (TEFs) for polycyclic aromatic hydrocarbons (PAHs), Regul. Toxicol. Pharm., 16, 290–300, https://doi.org/10.1016/0273-2300(92)90009-X, 1992.

Oros, D. R. and Simoneit, B. R. T.: Identification and emission rates of molecular tracers in coal smoke particulate matter, Fuel, 79, 515–536, https://doi.org/10.1016/S0016-2361(99)00153-2, 2000.

Paatero, P. and Hopke, P. K.: Discarding or downweighting high-noise variables in factor analytic models, Anal. Chim. Acta,

https://doi.org/10.5194/egusphere-2026-6761
Preprint. Discussion started: 11 November 2026
© Author(s) 2026. CC BY 4.0 License.

490, 277–289, https://doi.org/10.1016/s0003-2670(02)01643-4, 2003.

Ren, L., Fu, P., He, Y., Hou, J., Chen, J., Pavuluri, C. M., Sun, Y., and Wang, Z.: Molecular distributions and compound-specific stable carbon isotopic compositions of lipids in wintertime aerosols from Beijing, Sci. Rep., 6, 27481, https://doi.org/10.1038/srep27481, 2016.

Rogge, W. F., Hildemann, L. M., Mazurek, M. A., Cass, G. R., and Simoneit, B. R. T.: Sources of fine organic aerosol. 4. Particulate abrasion products from leaf surfaces of urban plants, Environ. Sci. Technol., 27, 2700–2711, https://doi.org/10.1021/es00049a008, 1993a.

Rogge, W. F., Mazurek, M. A., Hildemann, L. M., Cass, G. R., and Simoneit, B. R. T.: Quantification of urban organic aerosols at a molecular level: Identification, abundance and seasonal variation, Atmos. Environ. Part A-General Topics, 27, 1309–1330, https://doi.org/10.1016/0960-1686(93)90257-y, 1993b.

Simoneit, B. R. T., Elias, V. O., Kobayashi, M., Kawamura, K., Rushdi, A. I., Medeiros, P. M., Rogge, W. F., and Didyk, B. M.: Sugars-dominant water-soluble organic compounds in soils and characterization as tracers in atmospheric particulate matter, Environ. Sci. Technol., 38, 5939–5949, https://doi.org/10.1021/es0403099, 2004.

Song, T., Feng, M., Song, D., Zhou, L., Qiu, Y., Tan, Q., and Yang, F.: Enhanced nitrate contribution during winter haze events in a megacity of Sichuan Basin, China: Formation mechanism and source apportionment, J. Clean. Prod., 370, 133272, https://doi.org/10.1016/j.jclepro.2022.133272, 2022.

Sun, J., Shen, Z., Zhang, T., Kong, S., Zhang, H., Zhang, Q., Niu, X., Huang, S., Xu, H., Ho, K. F., and Cao, J.: A comprehensive evaluation of $PM_{2.5}$-bound PAHs and their derivative in winter from six megacities in China: Insight the source-dependent health risk and secondary reactions, Environ. Int., 165, 107344, https://doi.org/10.1016/j.envint.2022.107344, 2022.

Tian, Y., Liu, X., Huo, R., Shi, Z., Sun, Y., Feng, Y., and Harrison, R. M.: Organic compound source profiles of $PM_{2.5}$ from traffic emissions, coal combustion, industrial processes and dust, Chemosphere, 278, 130429, https://doi.org/10.1016/j.chemosphere.2021.130429, 2021.

Wang, G. H. and Kawamura, K.: Molecular characteristics of urban organic aerosols from Nanjing: A case study of a mega-city in China, Environ. Sci. Technol., 39, 7430–7438, https://doi.org/10.1021/es051055+, 2005.

Wang, G. H., Kawamura, K., Lee, S., Ho, K. F., and Cao, J. J.: Molecular, seasonal, and spatial distributions of organic aerosols from fourteen Chinese cities, Environ. Sci. Technol., 40, 4619–4625, https://doi.org/10.1021/es060291x, 2006.

Wang, G. H., Kawamura, K., Xie, M., Hu, S., Gao, S., Cao, J., An, Z., and Wang, Z.: Size-distributions of n-alkanes, PAHs and hopanes and their sources in the urban, mountain and marine atmospheres over East Asia, Atmos. Chem. Phys., 9, 8869–8882, https://doi.org/10.5194/acp-9-8869-2009, 2009.

https://doi.org/10.5194/egusphere-2026-6761
Preprint. Discussion started: 11 November 2026
© Author(s) 2026. CC BY 4.0 License.



Wang, J., Ho, S. S. H., Ma, S., Cao, J., Dai, W., Liu, S., Shen, Z., Huang, R., Wang, G., and Han, Y.: Characterization of $PM_{2.5}$ in Guangzhou, China: uses of organic markers for supporting source apportionment, Sci. Total Environ., 550, 961–971, https://doi.org/10.1016/j.scitotenv.2016.01.138, 2016.

Wang, Q., Jiang, N., Yin, S., Li, X., Yu, F., Guo, Y., and Zhang, R.: Carbonaceous species in $PM_{2.5}$ and PM_{10} in urban area of Zhengzhou in China: Seasonal variations and source apportionment, Atmos. Res., 191, 1–11, https://doi.org/10.1016/j.atmosres.2017.02.003, 2017.

Wang, T., Huang, R. J., Li, Y., Chen, Q., Chen, Y., Yang, L., Guo, J., Ni, H., Hoffmann, T., Wang, X., and Mai, B.: One-year characterization of organic aerosolmarkers in urban Beijing: Seasonal variation and spatiotemporal comparison, Sci. Total Environ., 743, 140689, https://doi.org/10.1016/j.scitotenv.2020.140689, 2020.

Wang, Y. S., Yao, L., Wang, L. L., Liu, Z. R., Ji, D. S., Tang, G. Q., Zhang, J. K., Sun, Y., Hu, B., and Xin, J. Y.: Mechanism for the formation of the January 2013 heavy haze pollution episode over central and eastern China, Sci. China Earth Sci., 57, 14–25, https://doi.org/10.1007/s11430-013-4773-4, 2014.

Yadav, K., Bhardwaj, A., and Sunder Raman, R.: Chemical characterization, source identification and potential health effects of $PM_{2.5}$-bound non-polar organic compounds over a COALESCE network site-Bhopal, India, Sci. Total Environ., 920, 170957, https://doi.org/10.1016/j.scitotenv.2024.170957, 2024.

Yamamoto, S. and Kawamura, K.: Compound-specific stable carbon and hydrogen isotopic compositions of n-alkanes in urban atmospheric aerosols from Tokyo, Geochem. J., 44, 419–430, https://doi.org/10.2343/geochemj.1.0084, 2010.

Yu, P., Xu, R., Huang, W., Yang, Z., Morawska, L., Johnston, F. H., Abramson, M. J., Knibbs, L., Marks, G. B., Heyworth, J., Kim, H., Tantrakarnapa, K., Kliengchuay, W., Matus, P., Hales, S., Lavigne, E., Saldiva, P. H. N., Coelho, M. S. Z. S., Ye, T., Yu, W., Liu, Y., Ju, K., Zhang, Y., Wu, Y., Wen, B., Guo, Y., and Li, S.: Contributions of traffic to daily $PM_{2.5}$ exposure and links to cancer mortality, Nat. Sustain., https://doi.org/10.1038/s41893-026-01925-5, 2026.

Zhang, J., Fu, X., Chen, C., Su, Y., Liu, S., Chen, L., Chen, Y., Wang, G., and Prevot, A. S. H.: Measurement report: Molecular composition, sources, and evolution of atmospheric organic aerosols in a basin city in China, Atmos. Chem. Phys., 25, 8983–9004, https://doi.org/10.5194/acp-25-8983-2025, 2025.

Zhang, J., Sun, W., Su, Y., Peng, X., Chen, C., Fu, X., Long, Y., Wang, G., Rao, Z., Han, L., and Huang, X.: Chemical composition, sources, and processes of winter haze in Chengdu, China: Insights from integrating the bulk chemical and single particle approaches, Atmos. Environ., 322, 120371, https://doi.org/10.1016/j.atmosenv.2024.120371, 2024a.

Zhang, J., Su, Y., Chen, C., Guo, W., Tan, Q., Feng, M., Song, D., Jiang, T., Chen, Q., Li, Y., Li, W., Wang, Y., Huang, X., Han, L., Wu, W., and Wang, G.: Chemical composition, sources and formation mechanism of urban $PM_{2.5}$ in Southwest China: a case study at the beginning of 2023, Atmos. Chem. Phys., 24, 2803–2820,

https://doi.org/10.5194/egusphere-2026-6761
Preprint. Discussion started: 11 November 2026
© Author(s) 2026. CC BY 4.0 License.



https://doi.org/10.5194/acp-24-2803-2024, 2024b.

Zhang, J., Zhou, Y., Yao, X., Zhao, W., Liu, S., Chen, Y., Shi, K., & Wang, G. (2026). data for "Measurement report: Molecular composition, size distribution, sources and evolution of organic aerosols in the Sichuan Basin, China–Part I: Non-polar organic compounds" [Dataset]. Zenodo. https://doi.org/10.5281/zenodo.23800734

Zhang, Y., Zheng, H., Zhang, L., Zhang, Z., Xing, X., and Qi, S.: Fine particle-bound polycyclic aromatic hydrocarbons (PAHs) at an urban site of Wuhan, central China: Characteristics, potential sources and cancer risks apportionment, Environ. Pollut., 246, 319–327, https://doi.org/10.1016/j.envpol.2018.11.111, 2019.